Title: The calcium-binding protein ALG-2 promotes endoplasmic reticulum exit site localization and polymerization of Trk-fused gene (TFG) protein

Author's name: Takashi Kanadome[1], Hideki Shibata[1], Keiko Kuwata[2], Terunao Takahara[1] and Masatoshi Maki[1]

Addresses: 1 Department of Applied Molecular Biosciences, Graduate School of Bioagricultural Sciences, Nagoya University, Japan
2 Institute of Transformative Bio-Molecules (WPI-ITbM), Nagoya University, Japan

Corresponding Author: H. Shibata, Department of Applied Molecular Biosciences, Graduate School of Bioagricultural Sciences, Nagoya University, Furo-cho, Chikusa-ku, Nagoya 464-8601, Japan
Fax: +81 52 789 5542
Tel: +81 52 789 5541
E-mail: shibabou@agr.nagoya-u.ac.jp

Running title: ALG-2 regulates TFG at ERES.

Abbreviations: ABM, ALG-2-binding motif; ALG-2, apoptosis-linked gene 2; ALIX, ALG-2-interacting protein X; CC, coiled-coil; DTSSP, 3,3-dithiobis-(sulfosuccinimidyl propionate); DTT, dithiothreitol; ERES, endoplasmic reticulum exit sites; FRAP, fluorescence recovery after photobleaching; GFP, green fluorescent protein; HEK, human embryonic kidney; PB1, Phox and Bem1; PEF, penta-EF-hand; PLSCR3, phospholipid scramblase 3; PQ-rich, proline/glutamine-rich; TFG, Trk-fused gene; TG, thapsigargin; TSG101, tumor susceptibility gene 101; VPS37C, vacuolar protein sorting-associated protein 37C.

Keywords: ALG-2; Ca^{2+}-binding protein; endoplasmic reticulum exit sites; protein-protein interaction; Trk-fused gene (TFG) protein

Abstract

Apoptosis-linked gene 2 (ALG-2), which is a gene product of *PDCD6*, is a 22-kDa Ca^{2+}-binding protein. Accumulating evidence points to a role for ALG-2 as a Ca^{2+}-responsive adaptor protein. On binding to Ca^{2+}, ALG-2 undergoes a conformational change that facilitates its interaction with various proteins. It also forms a homodimer and heterodimer with peflin, a paralog of ALG-2. However, the differences in cellular roles for the ALG-2 homodimer and ALG-2/peflin heterodimer are unclear. In the present study, we found that Trk-fused gene (TFG) protein interacted with the ALG-2 homodimer. Immunostaining analysis revealed that TFG and ALG-2 partially overlapped at endoplasmic reticulum exit sites (ERES), a platform for COPII-mediated protein transport from the endoplasmic reticulum. Time-lapse live-cell imaging demonstrated that both green fluorescent protein-fused TFG and mCherry-fused ALG-2 are recruited to ERES after thapsigargin treatment, which raises intracellular Ca^{2+} levels. Furthermore, overexpression of ALG-2 induced the accumulation of TFG at ERES. TFG has an ALG-2-binding motif and deletion of the motif decreased TFG binding to ALG-2 and shortened its half-life at ERES, suggesting a critical role for ALG-2 in retaining TFG at ERES. We also demonstrated, by *in vitro* cross-linking assays, that ALG-2 promoted the polymerization of TFG in a Ca^{2+}-dependent manner. Collectively, the results suggest that ALG-2 acts as a Ca^{2+}-sensitive adaptor to concentrate and polymerize TFG at ERES, supporting a potential role for ALG-2 in COPII-dependent trafficking from the endoplasmic reticulum.

Introduction

Ca^{2+} signaling is essential for various cellular events from fertilization to cell death as a second messenger [1]. The signaling is mediated mainly by Ca^{2+}-responsive proteins, such as calpains (Ca^{2+}-activated proteases) and calmodulin (a Ca^{2+}-binding protein). Apoptosis-linked gene 2 (ALG-2), which is a gene product of *PDCD6*, is a member of the family of penta-EF-hand Ca^{2+}-binding proteins that possess five serially repeated EF-hand motifs, or PEF domain [2]. Similar to calmodulin, ALG-2 interacts Ca^{2+}-dependently with various proteins including ALG-2-interacting protein X (ALIX) [3, 4], tumor susceptibility gene 101 (TSG101) [5], vacuolar protein sorting-associated protein 37C (VPS37C) [6], annexin A7 [7], annexin A11 [7, 8], phospholipid scramblase 3 (PLSCR3) [9], RBM22 [10] and Sec31A [11, 12]. By comparison with amino acid sequences of ALG-2-interacting regions in ALIX, PLSCR3 and Sec31A and their mutational analyses, two ALG-2-binding motifs (ABMs) have been identified so far: ABM-1 is represented as PPYP*X*nYP (*X*, variable; *n* = 4 in ALIX and PLSCR3) and ABM-2 is [PΦ]P*X*[PΦ]G[FW]Ω ([PΦ], Pro or hydrophobic; [FW], Phe or Trp; Ω, large side chain; *X*, variable) [9, 13-17]. X-ray crystal structure analyses of apo-ALG-2 and complexes of ALG-2/ALIX peptide [16] and

ALG-2/Sec31A peptide [17] have revealed that ALG-2 possesses three hydrophobic pockets designated as Pockets 1, 2 and 3. Pocket 1 and Pocket 2 are juxtaposed, and both serve as a binding site for ABM-1, whereas Pocket 3 provides a hydrophobic cavity that accepts ABM-2. This information has enabled *in silico* screening for novel ALG-2-interacting proteins [18]. Recently, CHERP has been characterized as an ALG-2-interacting protein and has been proposed to play a role in the regulation of alternative splicing of pre-mRNA in concert with ALG-2 [19].

Besides interacting with various proteins in a Ca^{2+}-dependent manner, ALG-2 forms a homodimer [3, 20, 21]. There is accumulating evidence that ALG-2 functions as a Ca^{2+}-responsive adaptor protein that bridges two proteins, such as ALIX and TSG101 in endocytosis [22] and Sec31A and annexin A11 in the early secretory pathway [23]. In addition, ALG-2 forms a heterodimer with peflin, a paralog of ALG-2 [21]. Peflin possesses a PEF domain similar to that of ALG-2 (40.9% identity) and a long N-terminal hydrophobic domain [24]. There is little information about the function of peflin and proteins that interact with peflin. The functional differences of ALG-2 in a homodimer and a heterodimer are also poorly understood.

In this study, we first investigated differences in proteins that interact in a Ca^{2+}-dependent manner with the ALG-2 homodimer and ALG-2/peflin heterodimer. Unfortunately, no protein interacting with the heterodimer was identified, although Trk-fused gene (TFG) protein was characterized as protein interacting with the homodimer. *TFG* was originally identified as a part of the thyroid oncogene *TRK-T3*, generated by a chromosomal rearrangement fusing with *NTRK1* (also named *TRKA*) in human papillary thyroid carcinoma [25]. *TFG* is a ubiquitously expressed gene in adult and fetal human tissues. Both ALG-2 and TFG proteins have been shown to localize at the endoplasmic reticulum exit sites (ERES)/transitional ER, from which COPII-coated vesicles emerge and bud off [11, 12, 26]. A recent studies by Johnson *et al*. [27] showed that TFG has the ability to self-assemble into an octameric complex and that the TFG complex generates larger polymers *in vitro*. In the present study, we characterized here the Ca^{2+}-dependent interaction of ALG-2 with TFG. An ABM-2-like sequence in the C-terminal proline/glutamine-rich (PQ-rich) region of TFG was required for the interaction. In addition, deletions and amino acid substitutions that perturb the self-assembly of TFG, including the SPG57 mutation in autosomal recessive spastic paraplegia (substitution of Arg^{106} with Cys, R106C) [28], abrogated the proper interaction with ALG-2. Indirect immunofluorescence and live-cell time-lapse analyses showed that ALG-2 promoted localization of TFG within ERES. Furthermore, based on an *in vitro* cross-linking study, we demonstrated that ALG-2 is important for polymerization of the TFG complex in a Ca^{2+}-dependent manner.

Results

TFG was identified as a Ca^{2+}-dependent interacting protein of the ALG-2 homodimer.

To determine differences in the functions of the ALG-2 homodimer and ALG-2/peflin heterodimer, we attempted to identify their specific interacting proteins by co-immunoprecipitation analysis. A key point in the experiment is that we used ALG-$2^{E47A/E114A}$, a mutant with two glutamate residues substituted for alanine in Ca^{2+}-coordinating positions of EF1 (E47A) and EF3 (E114A). It has been shown that the mutant is defective in Ca^{2+}-binding [20] and does not interact with Ca^{2+}-dependent binding partners, such as TSG101, ALIX and Sec31A [5, 12, 17]. Because the ALG-$2^{E47A/E114A}$ mutant has intact EF5 that is necessary for dimerization, it is to be expected that the mutant will form dimers with ALG-2 and peflin. FLAG-tagged ALG-$2^{E47A/E114A}$ (FLAG-ALG-$2^{E47A/E114A}$) and either nontagged ALG-2 or nontagged peflin were co-expressed in HEK293/ALG-2_{KD} cells in which endogenous ALG-2 had been depleted by shRNA-mediated RNA interference [22]. When FLAG-ALG-$2^{E47A/E114A}$ was immunoprecipitated from the cell lysate co-expressing nontagged ALG-2 with anti-FLAG antibody in the presence of 10 μM $CaCl_2$ and then eluted with a buffer containing 5 mM EGTA, a chelating agent for Ca^{2+}, several bands were detected in the eluate by SDS/PAGE and silver staining (Fig. 1A). Nontagged ALG-2, as well as FLAG-ALG-$2^{E47A/E114A}$, was found in the "Beads" fraction, which should include proteins not eluted by EGTA treatment from the beads. Therefore, as expected, the results suggested that nontagged ALG-2 could form a dimer with FLAG-ALG-$2^{E47A/E114A}$ and that the dimer would interact Ca^{2+}-dependently with proteins corresponding to these bands. By contrast, no significant band was detected in the EGTA-eluted fraction from the cell lysate expressing FLAG-ALG-$2^{E47A/E114A}$ and nontagged peflin, even though these proteins were detected in the "Beads" fraction. Several bands in the EGTA eluate from the cells expressing FLAG-ALG-$2^{E47A/E114A}$ and nontagged ALG-2 were excised from the gel and subjected to in-gel digestion by trypsin. The digested samples were analyzed by LC-MS/MS. As a result of a search in the Mascot database on the basis of LC-MS/MS data, we identified four proteins, Sec31A (Fig. 1A, band a1), TFG (Fig. 1A, band a2), TSG101 (Fig. 1A, band a3), and VPS37C (Fig 1A, band a4; Table S1). In previous studies, TSG101, VPS37C and Sec31A have been well characterized as ALG-2-interacting proteins [5, 6, 11, 12]. Although TFG has a sequence motif similar to the ALG-2 binding region of Sec31A (Fig. 2B) and direct interaction of ALG-2 with TFG had been shown by our far western analysis using biotin-labeled ALG-2 [18], further characterization of the interaction with ALG-2 was needed. In the present study, we focused on TFG and pursued the function of ALG-2 for TFG.

ALG-2 interacts with TFG in a Ca^{2+}-dependent manner.

First, to confirm the interaction between ALG-2 and TFG, we performed immunoprecipitation from HEK293 cell lysates using anti-TFG antibody and western blotting. Endogenous ALG-2 was detected in

the immuneprecipitates of anti-TFG antibody in the presence of $CaCl_2$ but not in the presence of EGTA (Fig. 1B). In reciprocal immunoprecipitation analysis with anti-ALG-2 antibody, endogenous TFG was co-immunoprecipitated with endogenous ALG-2 in a Ca^{2+}-dependent manner (Fig. 1C).

When protein samples were resolved by SDS-PAGE (7% and 8% gels), doublet bands were detected by the anti-TFG antibody used in this study and the upper band was dominant in HEK293 cells, as well as in HeLa cells. We also noticed that the doublet bands appeared to be stacked by using 12% SDS/PAGE gels (Fig. 2A). When cells were treated with siRNA duplexes against TFG mRNA, both signal levels corresponding to the doublet were reduced (data not shown). Additional work is necessary to address what is responsible for such a distinction in the mobility of endogenous TFG proteins.

ALG-2-binding motif 2 in the PQ-rich region of TFG.

Structural and biochemical studies have revealed the presence of two different modes of interactions between ALG-2 and its binding proteins [9, 16, 17]. A hydrophobic cavity of the ALG-2 molecule, consisting of Pocket 1 and Pocket 2, is responsible for the binding to proteins that have ABM-1 (ALG-2-binding motif 1), whereas Pocket 3 is the binding site for those containing another ALG-2-binding motif, ABM-2. To characterize the binding modes of ALG-2 and TFG, we performed a pulldown assay using GST-fused ALG-2 (GST-ALG-2) of the wild type (WT) and two mutants (Y180A and F85A). Y180 in Pocket 1 is critical for binding to proteins containing ABM-1, and F85 in Pocket 3 is critical for binding to proteins containing ABM-2 [17]. As shown in Fig. 2A, GST-ALG-2^{WT} pulled down TFG, Sec31A (a protein containing ABM-2) and ALIX (a protein containing ABM-1). The Y180A mutant failed to interact with ALIX but retained binding abilities toward TFG and Sec31A. On the other hand, the F85A mutant showed impairment in the interaction with both TFG and Sec31A without affecting the binding to ALIX. This result suggests that TFG, similar to Sec31A, is an ABM-2-containing protein. TFG possesses a sequence similar to ABM-2 in Sec31A at a position from P359 to F363 in its PQ-rich region (Fig. 2B). To address the significance of the ABM-2-like motif within TFG in the interaction with ALG-2, we performed a GST-ALG-2 pulldown assay using green fluorescent protein (GFP)-tagged TFG (GFP-TFG) of the WT and a mutant lacking the motif (ΔABM-2). Figure 2C shows that the interaction with GST-ALG-2 was largely compromised in the deletion mutant, suggesting that the ABM-2-like motif is required for the interaction. Because the deletion mutant had not completely lost its binding ability to GST-ALG-2, there might exist an ALG-2-binding site(s) other than the indicated ABM-2. The amount of endogenous Sec31A proteins in pulldown products was not altered by expression of GFP-TFG and GFP-$TFG^{\Delta ABM-2}$, whereas the amount of endogenous TFG in pulldown products was decreased by overexpression of GFP-TFG (Fig. 2C-E).

TFG has three distinct regions: Phox and Bem1 (PB1), coiled-coil (CC), and PQ-rich (Fig. 2B). We further examined the effect of deletions of these regions on the interaction with ALG-2 by using a GST-pulldown assay (Fig. 2D). Surprisingly, TFG mutants lacking PB1 (ΔPB1), CC (ΔCC) and the region of 1-155 amino acids (ΔNt) exhibited no or little interaction with ALG-2, even though they possess ABM-2. Taken together, these results suggest that ABM-2 in TFG is necessary but not sufficient for the proper interaction with ALG-2.

The neurodegenerative disorder-related TFG R106C mutation impairs the interaction with ALG-2.

Trk-fused gene has been identified as causative gene for neurodegenerative disorders [28, 29]. We investigated whether two neurodegenerative disorder-related mutations in TFG affect the interaction of ALG-2: P285L related to hereditary motor and sensory neuropathy with proximal dominance (HMSN-P) [29] and R106C related to hereditary spastic paraplegias (HSPs) [28] (Fig. 2B). In a GST-ALG-2 pulldown assay using GFP-TFG of the WT and mutants (P285L and R106C), the P285L mutant retained interaction with ALG-2 at a level comparable to that of WT, whereas the R106C mutant showed impaired interaction (Fig. 2E). Similar to the deletion mutants lacking the PB1 domain, CC domain and the N-terminal half (Figs. 2B,D), R106C possesses ABM-2. The N-terminal region of TFG containing PB1 and CC domains has been reported to play a role in formation of the oligomer [26]. R106 is located in the CC domain, and the R106C mutant has also been shown to have impairment of oligomerization [28]. Therefore, there is the possibility that the oligomerization ability of TFG may be necessary for proper interaction with ALG-2.

ALG-2 co-localizes with TFG at ERES.

Next, we performed triple immunostaining for TFG, ALG-2 and the COPII component Sec31A in HeLa cells. As shown in Fig. 3, immunofluorescence of ALG-2 was detected both in the nucleus and in the cytoplasm (Fig. 3B,E), while that of TFG and Sec31A was found in the cytoplasm as a punctate pattern (Fig. 3A,C,D,F). Merging of the images of ALG-2 and Sec31A showed a complete overlap between the two proteins in the cytoplasm (Fig. 3H). The punctate appearance of TFG staining resembled that of Sec31A and ALG-2. In the perinuclear cytoplasm, immunoreactive signals for TFG were strong and overlapped completely or partially with the ALG-2/Sec31A-positive structures (Fig. 3G,I,J). Outside the perinuclear area, TFG was detected at lower intensity as dot-like structures, many of which overlapped partially with the ALG-2/Sec31A-positive ones (Fig. 3G-J, arrows) and others exhibited no or little co-localization with ALG-2 and Sec31A (Fig. 3G-J, arrowheads). These observations suggest that TFG partially co-localized with ALG-2 at Sec31A-positive ERES.

We previously reported that ALG-2 functions as a Ca^{2+}-dependent adaptor protein mediating the indirect association between Sec31A and annexin A11 [23]. Because both TFG and Sec31A localize at ERES, it is conceivable that ALG-2 bridges the two proteins. To address this possibility, we performed a co-immunoprecipitation assay using HEK293 cells transiently expressing GFP-TFG and FLAG-ALG-2. As shown in Fig. 4, immunoprecipitation of GFP-TFG with anti-GFP antibody resulted in co-precipitation of FLAG-ALG-2 in the presence of Ca^{2+}, although endogenous Sec31A was not detected in the immunoprecipitated product. Therefore, there is no interaction between TFG and Sec31A and it is unlikely that ALG-2 can interact simultaneously with TFG and Sec31A.

By live-cell time-lapse imaging, ALG-2 has been shown to translocate from the cytosol to ERES in response to Ca^{2+} mobilization [15, 30]. To examine the effect of an increase in cytoplasmic Ca^{2+} on the subcellular distribution of TFG, HeLa cells expressing GFP-TFG and mCherry-fused ALG-2 (mCherry-ALG-2) were treated with thapsigargin (TG). TG is an inhibitor of SERCA (sarco/endoplasmic reticulum Ca^{2+} ATPase) and induces Ca^{2+} elevation in the cytosol. Before the administration of TG, GFP-TFG showed co-localization with mCherry-ALG-2 in a dot-like pattern in the cytoplasm (Fig. 5A,B, time 0). The number of GFP-TFG dots was not altered by the administration of TG, although the fluorescence levels of both proteins in the dots increased gradually. We traced the dot in the time-lapse images (as indicated by a white circle in Fig. 5B) and quantified the fluorescence intensities of both GFP-TFG and mCherry-ALG-2. The data showed a lag phase followed by a simultaneous increase and then a gradual decrease in the fluorescence intensities (Fig. 5C). Quantification of the GFP-TFG and mCherry-ALG-2 signal intensities at the area including one double-positive puncta for these fluorescent proteins revealed that administration of TG induced increases of 29% and 16% for GFP-TFG and mCherry-ALG-2, respectively (Fig. 5D). These observations suggest that TG treatment leads to recruitment of ALG-2 and TFG to ERES. To test the possibility that the increase in accumulation of both TFG and ALG-2 could be a result of ER stress induced by TG, we treated cells with dithiothreitol, another stimulator of ER stress. Administration of dithiothreitol had no consistent effect on intracellular Ca^{2+} levels (data not shown). As shown in Fig. 5E, the fluorescence intensities of GFP-TFG and mCherry-ALG-2 at their puncta were not significantly affected by the dithiothreitol treatment ($P = 0.74$ and $P = 0.21$, respectively). Therefore, elevation of cytosolic Ca^{2+} seems to be a major factor contributing to induce accumulations of GFP-TFG and mCherry-ALG-2 at ERES.

Overexpression of ALG-2 concentrates TFG at ERES.

To examine the role of ALG-2 in the subcellular localization of TFG, we performed immunostaining of endogenous TFG in HeLa cells that had been transfected with an expression construct of FLAG-ALG-

2 (WT) and FLAG-ALG-2$^{E47A/E114A}$ (E47A/E114A) (Fig. 6A). The cells expressing FLAG-ALG-2^{WT} (as indicated by plus signs) had strong fluorescent signals at the cytoplasmic puncta compared to cells with no signal for FLAG-ALG-2^{WT} (as indicated by minus signs). By contrast, no apparent differences in the fluorescent signals of TFG were observed in cells expressing FLAG-ALG-2$^{E47A/E114A}$. Quantification of the fluorescent signal intensity of TFG revealed that expression of FLAG-ALG-2^{WT} caused a statistically significant increase (more than two times) in TFG signals at the cytoplasmic puncta. We also examined the effect of overexpression of ALG-2 on the subcellular localization of Sec31A. By contrast to the case of TFG-positive structures, neither FLAG-ALG-2^{WT} nor FLAG-ALG-2$^{E47A/E114A}$ had a significant effect on the fluorescent intensities of Sec31A (Fig. 6B). To rule out the possibility that TFG is upregulated by the expression of FLAG-ALG-2^{WT}, western blotting was performed. The results showed that expression levels of TFG and Sec31A were not altered in cells transfected with the expression construct of FLAG-ALG-2^{WT} and FLAG-ALG-2$^{E47A/E114A}$ (Fig. 6C, left). Upregulation of a molecular chaperone BiP/GRP78 and reduction of full-length ATF6α [pATF6α(P)/p90ATF6α] are hallmarks of ER stress [31, 32] (Fig. 6C, right). Overexpression of FLAG-ALG-2^{WT} or FLAG-ALG-2$^{E47A/E114A}$ had little effect on the protein levels of BiP or pATF6α(P) (Fig. 6C, left). Therefore, it is unlikely that the increased levels of TFG at ERES in ALG-2-overexpressing cells are associated with ER stress. We confirmed, by an immunoprecipitation assay using anti-FLAG antibody that FLAG-ALG-2^{WT}, but not FLAG-ALG-2$^{E47A/E114A}$, had binding ability to TFG and Sec31A (Fig. 6D). Furthermore, we examined the effect of RNAi-mediated ALG-2-silencing on the localization of TFG in ERES in HeLa cells (Fig. 6E). Immunofluorescence analysis showed no detectable difference in fluorescence intensity of TFG at ERES between control and ALG-2-silencing cells. Together, these results suggest that ALG-2 is not required for localization of TFG to ERES but promotes accumulation of TFG at ALG-2-positive structures probably via the Ca^{2+}-dependent function of ALG-2.

ABM-2 is important for the retention of TFG at ERES.

To further investigate the role of ABM-2 of TFG in subcellular dynamics, fluorescence recovery after photobleaching (FRAP) experiments were performed in HeLa cells expressing GFP-TFG^{WT} and GFP-TFG$^{\Delta ABM-2}$. Both proteins were observed as a punctate pattern in the cytoplasm (Fig. 7A). When the cells were processed for immunofluorescence staining with anti-Sec31A antibody, the cytoplasmic punctate structures labeled with GFP-TFG^{WT} and GFP-TFG$^{\Delta ABM-2}$ overlapped the Sec31A-positive puncta. Therefore, the GFP-positive structures could be defined as ERES. As found in a previous study [27], GFP-TFG^{WT} was also observed as abnormally large granules in some cells (Fig. 7B). ALG-2 was accumulated in the large TFG structures. In the FRAP experiments, we selected cells with a punctate pattern of GFP-

TFG^{WT} and GFP-$TFG^{\Delta ABM\text{-}2}$ similar to the distribution of endogenous TFG. A region including a GFP-positive dot was photobleached, and recovery of GFP fluorescence was followed (Fig. 7C). Relative recovery rates in multiple cells were averaged and plotted as a function of time (Fig. 7D). The kinetics of recovery was markedly altered by the deletion of ABM-2, and the maximum recovery rate was higher in GFP-$TFG^{\Delta ABM\text{-}2}$ than in GFP-TFG^{WT}. The half-time of fluorescence recovery ($t_{1/2}$) was determined by fitting of the experimental data to a single exponential. Statistical analysis revealed that the half-time of GFP-$TFG^{\Delta ABM\text{-}2}$ was significantly shortened and that ABM-2 deletion reduced the immobile population to almost half (Table 1). These data indicate that ABM-2 has an impact on the stable retention of TFG at ERES.

ALG-2 facilitates the polymerization of TFG *in vitro*.

The results of several *in vitro* studies have indicated that TFG exists as an octameric cup-like structure that is capable of self-assembly to form larger polymers [27]. We found that ALG-2 binds Ca^{2+}-dependently to TFG and that cytosolic Ca^{2+} elevation and ALG-2 overexpression lead to accumulation of TFG at ERES. These findings prompted us to examine whether ALG-2 promotes the formation of the octamer and/or polymer of TFG. We prepared recombinant His-tagged TFG proteins (TFG-His) expressed in *Escherichia coli* and performed an *in vitro* cross-linking assay using the chemical cross-linker DTSSP 3,3-dithiobis-(sulfosuccinimidyl propionate) (DTSSP), which is cleavable under a reduced condition. First, to determine the assembly state of recombinant TFG-His, the proteins were incubated with increasing concentrations of DTSSP (0.01-5 mM), resolved by SDS-PAGE under nonreducing and reducing conditions, and analyzed by western blotting with anti-TFG antibody (Fig. 8). In the absence of DTSSP, both nonreduced and reduced TFG-His proteins were detected as a single band that migrated at a molecular mass of approximately 57 000 corresponding to a monomeric form on SDS/PAGE. Under a nonreducing condition (Fig. 8, upper), the intensity of the band was decreased by incubation with 0.1 mM DTSSP and the band disappeared completely by treatment with DTSSP at concentrations greater than 0.5 mM, whereas new bands with molecular masses higher than 220 000 were detected as a broad pattern by treatment with 0.2 mM DTSSP. The new broad bands were increased in intensity and shifted to narrow bands as the concentration of DTSSP was increased (0.5-5 mM). Under a reduced condition (Fig. 8, lower), there was no band with a molecular mass higher than 220 000. Instead, the band detected in the absence of DTSSP (as indicated by a filled arrowhead) was shifted to a single band with slightly slower mobility (as indicated by an open arrowhead) in a concentration-dependent manner by DTSSP, indicating that TFG-His proteins are modified by DTSSP. As a result of treatment with 1 mM DTSSP, almost all of the TFG-His proteins appeared to have been modified in our experimental conditions. These results suggest that recombinant

TFG-His exists as a stable homo-oligomer *in vitro* (probably an octamer) [27].

Next, we examined the effect of ALG-2 on polymerization of TFG. To avoid aggregation of recombinant ALG-2 in the *in vitro* assay, we used the recombinant truncated form of ALG-2 that lacks the N-terminal hydrophobic region (des3-20ALG-2) [16]. TFG-His was co-immunoprecipitated with the recombinant des3-20ALG-2 in the presence of $CaCl_2$ but not in the presence of EGTA, indicating Ca^{2+}-dependent direct interaction between the two recombinant proteins (Fig. 9A). To investigate the effect of the interaction with ALG-2 on assembly state of TFG, TFG-His was incubated with des3-20ALG-2 proteins in the presence of EGTA or $CaCl_2$, and then the mixture was treated with 1 mM DTSSP. As shown in the upper panel of Fig. 9B, western blotting with anti-TFG antibody showed that the bands with high mobility under a non-reduced condition were gradually diminished by the addition of an increasing amount of ALG-2 in the presence of $CaCl_2$, but not in the presence of EGTA, with concomitant appearance of a band that remained just below or at the well bottom in the stacking gel (indicated by an arrow). There was no effect of ALG-2 on mobility of TFG-His proteins under a reduced condition (Fig. 9B, lower). Consistent with the mobility shift of TFG-His, ALG-2 proteins were also detected near the wells in the presence of $CaCl_2$ (Fig. 9C, upper). In the absence of Ca^{2+}, ALG-2 proteins were detected only as a single band corresponding to the approximate molecular mass of a homodimer (~ 40 000). When the ALG-2 proteins were incubated with DTSSP in the absence of TFG-His, there was no band near the wells in either the EGTA or $CaCl_2$ conditions (Fig. 9D, arrows). These results clearly indicate that ALG-2 bridges the TFG oligomer to facilitate its polymerization in a Ca^{2+}-dependent fashion.

To further confirm the role of ALG-2 in the polymerization of TFG, we prepared two mutants of TFG-His: a deletion mutant, $TFG^{\Delta ABM\text{-}2}$-His, and a substitution mutant, TFG^{R106C}-His. As described above, these mutations caused reduction in ALG-2 binding in our GST-ALG-2 pulldown analysis (Fig. 2C,E). We first examined the oligomeric state of the mutant proteins by treatment with an increasing concentration of DTSSP. Under nonreduced and reduced conditions, the pattern in band shifts seen with $TFG^{\Delta ABM\text{-}2}$-His was similar to the WT (Fig. 10A), suggesting no effect of the ABM-2 deletion on oligomer formation of TFG. By contrast, the R106C mutation resulted in the appearance of faster and broader bands in mobility under a nonreduced condition when the proteins were incubated with DTSSP at concentrations greater than 0.5 mM (Fig. 10B, upper). The modification of TFG^{R106C}-His by DTSSP appeared to occur to an extent similar to that of TFG^{WT}-His and $TFG^{\Delta ABM\text{-}2}$-His, because the pattern in band shift of TFG^{R106C}-His was similar to that seen in TFG^{WT}-His and $TFG^{\Delta ABM\text{-}2}$-His under a reduced condition (Fig. 10B, lower). These results indicate that the R106C mutant retains the ability to form an oligomer but that the resultant TFG^{R106C}-His oligomers display a perturbed architecture *in vitro*. This is consistent with the results of previous studies showing a defect in the ability of the mutant to self-assemble into an octamer based on

its hydrodynamic and light scattering properties [28]. Next, we examined the effect of ALG-2 on polymerization of TFG-His mutants. Compared with the pattern in the band shift of TFG^{WT}-His from oligomeric to polymeric forms (Fig. 10C, upper left), the bands corresponding to the $TFG^{\Delta ABM\text{-}2}$-His oligomer were also reduced in intensity by incubation with an increasing concentration of ALG-2 but to a lesser extent. The reduction of the broader bands corresponding to abnormal oligomers of TFG^{R106C}-His appeared to be comparable to that observed in the WT. Western blotting with anti-ALG-2 antibody (Fig. 10C, right) demonstrated that the ALG-2 proteins were incorporated into the TFG^{R106C}-His polymers as well as the TFG^{WT}-His polymers (indicated by an arrow). By contrast, bands in mobility at the oligomeric form of TFG were predominantly detected in the case of $TFG^{\Delta ABM\text{-}2}$-His. These results suggest that des3-20ALG-2 could bind to both $TFG^{\Delta ABM\text{-}2}$-His and TFG^{R106C}-His in this experimental condition, probably as a result of the high concentrations of the proteins used. Although the TFG^{R106C}-His oligomer and the $TFG^{\Delta ABM\text{-}2}$-His oligomer appeared to assemble into polymers in the presence of ALG-2, the relative decrease in the intensity of bands corresponding to each oligomer with increasing ALG-2 concentration indicates that ABM-2 deletion causes a significant decrease in the ALG-2-promoted polymerization of TFG (Fig. 10D).

Discussion

ALG-2 has been shown to stabilize a COPII component, Sec31A, at ERES and to participate in processes involving anterograde transport from the ER to the Golgi apparatus [11, 23, 33, 34]. ALG-2 forms a homodimer or a heterodimer with peflin [3, 20, 21]. Although there is accumulating evidence indicating that ALG-2 interacts with various proteins [35], there have been only a few reports of proteins interacting with peflin [36, 37]. During the preparation of this manuscript, Rayl et al. reported that peflin is a negative regulator of the ER-to-Golgi transport by suppressing the interaction between ALG-2 and Sec31A [38]. In the present study, we found several proteins that interact Ca^{2+}-dependently with the dimer of FLAG-ALG-$2^{E47A/E114A}$/ALG-2 by immunoprecipitation with anti-FLAG antibody (Fig. 1A). By contrast, there was no band corresponding to candidate proteins that specifically bind to the FLAG-ALG-$2^{E47A/E114A}$/peflin heterodimer. It remains unclear whether the ALG-2/peflin heterodimer interacts with Sec31A and/or with other unknown proteins to regulate ER-to-Golgi transport.

Our recent structural analyses have revealed that each ALG-2 molecule in its homodimer has two binding sites, each of which interacts with one of the two ALG-2 binding motifs: ABM-1 and ABM-2 [16, 17, 39]. Because there are at least four binding sites in an ALG-2 homodimer, it is proposed that ALG-2 functions as a Ca^{2+}-dependent adaptor protein [35, 40]. We previously demonstrated that ALG-2 bridges annexin A11 and Sec31A via the adaptor function and that annexin A11 is required for stabilization of

Sec31A on the membranes of ERES [23]. Because TFG binds to ALG-2 with characteristics of ABM-2-containing proteins (Fig. 2) and co-localizes substantially at ALG-2/Sec31A-positive structures (Figs. 3, 5, 6 and 7), it was expected that ALG-2 would mediate the association between Sec31A and TFG; however, this was not observed in our immunoprecipitation analysis (Fig. 4). Therefore, ALG-2 may have divergent functions at ERES via its mutually exclusive interaction with either Sec31A or TFG.

Immunofluorescence staining analysis demonstrated that overexpression of ALG-2 leads to enrichment of TFG in ERES without any effect on the distribution of Sec31A (Fig. 6A,B). By contrast, knockdown of ALG-2 has no significant effect on localization of TFG to ERES (Fig. 6E), suggesting that ALG-2 is not required for recruitment of TFG to ERES under normal culture conditions. Translocation of TFG to ERES might be a prerequisite step for the Ca^{2+}-dependent interaction with ALG-2. Luminal Ca^{2+} has been shown to play a regulatory role in ER-to-Golgi transport, in which ALG-2 is considered to be a sensor for released luminal Ca^{2+} [41, 42]. Therefore, it was conceivable that synchronous transport of cargo proteins affected the co-localization pattern between ALG-2 and TFG. To address this, we monitored immunofluorescence signals of ALG-2 and TFG along with transport of a model cargo protein, VSV-G tsO45 (a temperature-sensitive variant of vesicular stomatitis virus glycoprotein), from the ER to the cell surface in HT1080 cells constitutively expressing GFP-fused VSV-G tsO45 (tsO45 G-GFP) [23]. However, we were not able to find detectable differences in fluorescence intensities and in distribution patterns of ALG-2 and TFG at any time point after the temperature shift (data not shown). Nonetheless, live-cell time-lapse imaging showed that ALG-2 and TFG are accumulated in the cytoplasmic puncta, probably representing ERES, in response to Ca^{2+} mobilization (Fig. 5). Accumulation of GFP-TFG after treatment of TG was not observed in both ALG-2-depleted cells and cells without co-expression of mCherry-ALG-2 (data not shown). In addition, the Ca^{2+}-dependent binding of ALG-2 to TFG promotes TFG polymerization *in vitro* (Figs. 9 and 10). Taken together, the results suggest that a substantial amount of ALG-2 locally concentrates TFG at ERES probably under conditions of Ca^{2+} overload and under some disease conditions such as lung and mesenchymal tumors, in which ALG-2 is upregulated [43, 44].

Previous three-dimensional electron microscopic analysis revealed that TFG proteins homooligomerize to form octameric cup-like structures [27]. The PB1 and CC domains are sufficient for formation of the octamer. Meanwhile, the C-terminal PQ-rich region was shown to be responsible for further polymerization of the octameric TFG complexes under optical ionic conditions [27]. An *in vitro* cross-linking assay showed a potential role of ALG-2 in the architecture of TFG. Because the recombinant TFG proteins appeared to form a stable oligomer under the condition used (Fig. 8), we are not able to evaluate the contribution of ALG-2 to the oligomer formation of TFG. On the other hand, several results indicate that ALG-2 binds to the TFG oligomer to form a polymeric structure. First, ALG-2 was found to

react with the TFG oligomer in a stoichiometric manner in the presence of Ca^{2+} (Figs. 9B and 10C,D). Second, ALG-2 was incorporated into the TFG polymer (Figs. 9C and 10C). Third, a deletion mutant lacking ABM-2 showed no abnormality in its oligomer formation but a reduced ability to polymerize in response to ALG-2 (Fig. 10A,C,D). Finally, our GST-ALG-2 pulldown assay demonstrated no or little interactions of ALG-2 with TFG mutants that affect its ability to oligomerize (Fig. 2D,E) [28, 45]. Based on these results, we propose that ALG-2 promotes polymerization of the TFG octamer via its adaptor function. Because the PQ-rich region of TFG is capable of self-assembly [27], it is possible that ALG-2 stabilizes the assembled TFG complex in a Ca^{2+}-dependent manner.

Witte *et al*. [26] previously reported TFG-1, a *Caenorhabditis elegans* ortholog of TFG, as one of the interaction proteins for *C. elegans* SEC-16. It was further demonstrated that an interaction between human TFG and Sec16B. Sec16 proteins serve as a scaffold at ERES. To explore the role of Sec16 isoforms in the association between ALG-2 and TFG, we performed immunoprecipitation with anti-FLAG antibody from cell lysate of HEK293 cells expressing FLAG-ALG-2 followed by immunoblotting with antibodies against TFG, Sec16A, and Sec16B [46, 47]. Endogenous TFG was found in the immunoprecipitates of FLAG-ALG-2 in the presence of 100 μM $CaCl_2$, whereas no or undetectable levels of Sec16A or Sec16B were present in the immunoprecipitates of FLAG-ALG-2 (data not shown). Thus, it is unlikely that these Sec16 isoforms are involved in Ca^{2+}-dependent association between ALG-2 and TFG.

Although it is clear that TFG localizes to ERES, it remains controversial whether TFG has a general role in ER-to-Golgi transport. A transport assay using tsO45 G-GFP has demonstrated a substantial delay in the exit of cargo proteins from the ER in TFG-depleted HeLa cells [26]. Golgi reassembly following brefeldin A washout was also delayed in TFG-depleted RPE-1 cells [27]. By contrast, another assay using the RUSH (retention using selective hooks) system has shown unperturbed ER-to-Golgi transport of several cargoes, including a truncated form of mannosidase II, a non-temperature-sensitive variant of VSV-G, E-cadherin and galactosyl transferase [48]. In IMR-90 fibroblasts, it was reported that depletion of TFG leads to retention of procollagen I in the ER, indicating a specific role of TFG in the transport of procollagen [48]. Some of these discrepancies might be a result of the different experimental conditions, in which cells are probably subject to different levels of stress arising from accumulated cargo proteins in the ER, and/or a result of variations in the expression level of ALG-2. ALG-2 might confer tolerance to the stress by changing the architecture of TFG from the oligomeric state to the polymeric state. Although overexpression of both ALG-2 and TFG did not affect the transport of tsO45 G-GFP and the distribution of the cis-Golgi compartment stained with anti-GM130 antibody (data not shown), proteomic analysis of proteins secreted from cells with high expression of ALG-2 may provide further insights into the role of the interaction between ALG-2 and TFG in ERES.

Materials and Methods

Antibodies

The following commercially available antibodies were used: rabbit monoclonal antibody against TFG (ab156866; Abcam, Cambridge, MA, USA); mouse monoclonal antibody against FLAG (clone M2), rabbit polyclonal antibody against FLAG (F7425) and mouse monoclonal antibody against α-tubulin (clone DM1A; Sigma-Aldrich, St Louis, MO, USA); mouse monoclonal antibodies against Sec31A for immunostaining (clone 32) and BiP/GRP78 for Western blotting (clone 40/BiP; BD Transduction Laboratories, Franklin Lakes, NJ, USA); mouse monoclonal antibody against ALG-2 for immunoprecipitation (clone 2BA; Abnova, Taipei, Taiwan); rabbit polyclonal antibody against ALIX (CVL-PAB0204; Covalab, Villeurbanne, France); mouse monoclonal antibody against GFP (clone B2, sc-9996; Santa Cruz Biotechnology, Santa Cruz, CA, USA); rabbit polyclonal antisera against GFP for immunoprecipitation (A6455; Invitrogen/Molecular Probes, Carlsbad, CA, USA); and mouse monoclonal antibody against ATF6α for western blotting (clone 1-7; BioAcademia, Osaka, Japan). Rabbit polyclonal antibodies against Sec16A and Sec16B were kindly provided by the late K. Tani and Y. Maemoto (Tokyo University of Pharmacy and Life Science, Tokyo, Japan) [46, 47]. The following antibodies were raised as described previously: rabbit polyclonal antibody against ALG-2 for western blotting [12], goat polyclonal antibody against ALG-2 for immunostaining [18], and rabbit polyclonal antibody against Sec31A for western blotting and immunostaining [23].

Plasmid construction

pSGFP2-C1/TFG was constructed as follows: full-length TFG (NM_001007565.2.) was amplified from an HEK293 cDNA library (Clontech, Palo Alto, CA, USA) by PCR with a pair of primers (forward: 5'-CTCAAGCTTCGAATTCCACCATGAACGGACAGTTG-3'; reverse: 5'-CCGCGGTACCGTCGACCTTATCGATAACCAGGTCC-3'). The product was inserted into the *Eco*RI- and *Sal*I-digested pSGFP2-C1 vector (kindly provided by I. Wada, Fukushima Medical University, Japan) using an In-Fusion Advantage PCR Cloning Kit (Clontech). pSGFP2-C1/TFG$^{\Delta ABM-2}$ (Δ359-363), pSGFP2-C1/TFG$^{\Delta PB1}$ (Δ10-91), pSGFP2-C1/TFG$^{\Delta CC}$ (Δ92-124), pSGFP2-C1/TFG$^{\Delta Ct}$ (Δ156-400, substitution of the Q156 codon with a stop codon), pSGFP2-C1/TFG^{R106C}, and pSGFP2-C1/TFG^{P285L} were obtained by PCR-based site-directed mutagenesis using pSGFP2-C1/TFG as a template and pairs of primers: ΔABM-2 (forward: 5'-CCTGGGGCCTATCAAACTTCACTTCCTGG-3'; reverse: 5'-CCAGGAAGTGAAGTTTGATAGGCCCCAGG-3'), ΔPB1 (forward: 5'-GGATCTAAGTGGGGGCCAGCCAAGACC-3'; reverse: 5'-

GGTCTTGGCTGGCCCCCACTTAGATCC-3'), ΔCC (forward: 5'-CATTATTTGTTAATCCACCTGGAGAACC-3'; reverse: 5'-GGTTCTCCAGGTGGATTAACAAATAATG-3'), ΔCt (forward: 5'-GATTCTTCTGGAAAATAGTCTACTCAGG-3'; reverse: 5'-CCTGAGTAGACTATTTTCCAGAAGAATC-3'), R106C (forward: 5'-CAGGTGAAATATCTCTGTCGAGAACTGATAG-3'; reverse: 5'-CTATCAGTTCTCGACAGAGATATTTCACCTG-3') and P285L (forward: 5'-CTGGACCTCAACAACTTCAGCAGTTCCAGG-3'; reverse: 5'-CCTGGAACTGCTGAAGTTGTTGAGGTCCAG-3'). pSGFP2-C3/TFG$^{\Delta Nt}$ (Δ1-155) was obtained by inserting *Eco*RI- and *Sal*I-digested pEGFP-C3/TFG $^{\Delta 1\text{-}155}$ into the *Eco*RI- and *Sal*I-digested pSGFP2-C3 vector [18]. pcDNA3/peflin^{WT} was obtained by inserting *Eco*RI- and *Sal*I-digested pCMVTag2B/peflin [21] into the *Eco*RI- and *Xho*I-digested pcDNA3 vector. pCMVTag2A/ALG-2$^{E47A/E114A}$ RNAi^{R} was obtained by introducing a silent mutation within the RNAi-responsible sequence of pCMVTag2A/ALG-2$^{E47A/E114A}$ [13] using a pair of primers (forward: 5'-GAGGGTCGATAAAGACAGatcTGGcGTGATATCAGACACCGAG-3'; reverse: 5'-CTCGGTGTCTGATATCACgCCAgatCTGTCTTTATCGACCCTC-3').

A bacterial expression plasmid, pET24d/TFG-6xHis, was constructed as follows: the DNA fragment encoding TFG was amplified using pSGFP2-C1/TFG as a template and a pair of primers (forward: GGAGATATTACCATGAACGGACAGTTGGATCTAAG-3'; reverse: 5'-GGTGGTGGTGCTCGAGTCGATAACCAGGTCCAGGTT-3'). The product was inserted into the *Nco*I- and *Xho*I-digested pET24d vector using an In-Fusion Advantage PCR Cloning Kit (Clontech). Plasmids encoding the mutants, pET24d/TFG$^{\Delta ABM\text{-}2}$-6xHis and pET24d/TFG^{R106C}-6xHis, were obtained by PCR-based site-directed mutagenesis using pET24d/TFG-6xHis as a template and the pairs of primers shown above.

pCMVTag2A/ALG-2^{WT} RNAi^{R} [22], pcDNA3/ALG-2^{WT} RNAi^{R} [49] and pmCherry-ALG-2 [19] were constructed as described previously.

Cell culture and DNA transfection

HEK293 cells, HEK293/ALG-2$_{KD}$ cells [22] and HeLa cells were cultured in DMEM (Nissui, Tokyo, Japan) supplemented with 5% or 10% fetal bovine serum, 4 mM $_{L}$-glutamine, 100 U/mL penicillin and 100 μg/mL streptomycin at 37ºC under humidified air containing 5% CO_2. HEK293 cells and HEK293 ALG-2$_{KD}$ cells were transfected with plasmids using the conventional calcium phosphate method. HeLa cells were transfected with plasmids using FuGENE 6 (Promega, Madison, WI, USA).

Exploration of ALG-2/ALG-2 or ALG-2/peflin-interacting proteins

HEK293/ALG-2_{KD} cells co-transfected with pCMVTag2A/ALG-$2^{E47A/E114A}$ $RNAi^{R}$ and pcDNA3/ALG-2^{WT} $RNAi^{R}$ or pcDNA3/$peflin^{WT}$ were lysed in a lysis buffer (20 mM Hepes-NaOH, pH 7.4, 142.5 mM KCl, 1.5 mM $MgCl_2$, 10 μM $CaCl_2$, 1% Chaps) containing protease inhibitors (3 μg/ml leupeptin, 0.1 mM Pefabloc, 1 μM pepstatin A, 1 μM E-64, 0.2 mM phenylmethanesulfonyl fluoride) and phosphatase inhibitors (50 mM NaF, 10 mM β-glycerophosphate, 1 mM Na_3VO_4) and incubated on ice for 30 min. After centrifugation at 12 000 *g* for 10 min at 4°C, the cleared cell lysates were incubated with anti-FLAG antibody overnight at 4°C. Then the lysates were incubated with Dynabeads Protein G (Invitrogen) for 2 h at 4°C. The beads were washed with the lysis buffer three times and incubated with an elution buffer (20 mM Hepes-NaOH, pH 7.4, 142.5 mM KCl, 1.5 mM $MgCl_2$, 5 mM EGTA, 1% Chaps). The bound proteins were subjected to SDS/PAGE followed by silver staining. Specific bands were excised and digested in gel using Trypsin/Lys-C Mix (Promega). The peptides were analyzed by Triple TOF 5600+ (AB Sciex, Framingham, MA, USA).

MS and chromatographic methods, instrumentations and database searches

Samples were analyzed by nano-flow reverse phase liquid chromatography followed by tandem MS, using a Triple TOF 5600+, essentially described as previously [50]. Briefly, a capillary reverse phase HPLC-MS/MS system composed of an Eksigent Ekspert nano-LC 400 HPLC system (AB Sciex), which was directly connected to an AB Sciex quadrupole time-of-flight (QqTOF) TripleTOF 5600+ mass spectrometer in Trap and Elute mode. In the Trap and Elute mode, samples were automatically injected using Ekspert 400 system into a peptide trap column (ChromeXP, C18-CL, 200 μm inner diameter x 0.5 mm, 3 μm particle size, 120 Å pore size; AB Sciex) attached to a cHiPLC system (AB Sciex) for desalinating and concentrating peptides. After washing the trap with MS-grade water containing 0.1% trifluoroacetic acid and 2% acetonitrile (solvent C), the peptides were loaded into a separation capillary C18 reverse phase column (NTCC-360/100-3-125, 125 × 0.1 mm; Nikkyo Technos, Tokyo, Japan) by switching the valve. The eluents used were: (A) 100% water containing 0.1% formic acid, and (B) 100% acetonitrile containing 0.1% formic acid. The column was developed at a flow rate of 0.5 μL/min with the concentration gradient of acetonitrile: from 2% **B** to 32% **B** in 100 min, 32% **B** to 80% **B** in 1 min, sustaining 80% **B** for 10 min, from 80% **B** to 2% **B** in 1 min, and finally re-equilibrating with 2% **B** for 15 min. Mass spectra and tandem mass spectra were recorded in positive-ion and "high-sensitivity" mode with a resolution of approximately 35 000 full-width half-maximum. The nanospray needle voltage was typically 2300 V in HPLC-MS mode. After acquisition of approximately 6 samples, TOF MS spectra and

TOF MS/MS spectra were automatically calibrated during dynamic LC-MS & MS/MS autocalibration acquisitions injecting 50 fmol BSA. An Analyst TF1.6 system (AB Sciex) was used to record peptide spectra over the mass range of *m/z* 400–1250, and MS/MS spectra in information-dependent data acquisition (IDA) over the mass range of *m/z* 100–1600. For CID-MS/MS, the mass window for precursor ion selection of the quadrupole mass analyzer was set to 0.7 ± 0.1 Da. The precursor ions were fragmented in a collision cell using nitrogen as the collision gas. IDA was used for MS/MS collection on the TripleTOF 5600+ to obtain MS/MS spectra for the 20 most abundant parent ions following each survey MS1 scan (acquisition time of 250 msec per MS1 scan and a typical acquisition time of 100 msec per each MS/MS). Dynamic exclusion features were based on value *m/z* and were set to an exclusion mass width 50 mDa and an exclusion duration of 12 s.

Searches were performed by using MASCOT, version 2.4.0 (Matrix Science, Boston, MA, USA) against latest *Homo sapiens* (human, TaxID = 9606) Swissprot database for protein identification. Searching parameters were set as: enzyme selected as used with three maximum missing cleavage sites, species limited to *H. sapiens*, a mass tolerance of 45 p.p.m. for peptide tolerance, 0.1 Da for MS/MS tolerance, fixed modification of propionamide (C) and variable modification of oxidation (M). The maximum expectation value for accepting individual peptide ion scores [$-10 \times \mathrm{Log}(P)$] was set to ≤ 0.05, where P is the probability that the observed match is a random event. Protein identification and modification information returned from MASCOT were manually inspected and filtered to obtain confirmed protein identification and modification lists of CID MS/MS.

Immunoprecipitation

HEK293 cells were lysed in a lysis buffer [20 mM Hepes-NaOH, pH 7.4, 142.5 mM KCl, 1.5 mM $MgCl_2$, 1% (for immunoprecipitation with anti-ALG-2 antibody) or 0.3% (for immunoprecipitation with anti-TFG antibody) Chaps] containing the protease inhibitors and phosphatase inhibitors stated above and incubated on ice for 30 min. After centrifugation at 12 000 *g* for 10 min at 4°C, the cleared cell lysates were incubated with antibodies in the presence of 5 mM EGTA or 100 μM $CaCl_2$ overnight at 4°C. Then the lysates were incubated with Dynabeads Protein G for 2 h at 4°C. The beads were washed with lysis buffer containing 5 mM EGTA or 100 μM $CaCl_2$ three times and processed for sample preparation.

GST-ALG-2 pulldown

HEK293 cells transiently transfected with expression plasmids for GFP and GFP-fused proteins were lysed in a lysis buffer (20 mM Hepes-NaOH, pH 7.4, 142.5 mM KCl, 1.5 mM $MgCl_2$, 1% Chaps) containing the protease inhibitors and phosphatase inhibitors stated above and incubated on ice for 30 min.

After centrifugation at 12 000 *g* for 10 min at 4°C, the cleared cell lysates were incubated with Glutathione Sepharose 4B (GE Healthcare, Little Chalfont, UK) immobilizing GST-fusion proteins in the presence of 10 μM $CaCl_2$ for 2 h at 4°C. The beads were washed with lysis buffer containing 10 μM $CaCl_2$ three times and processed for sample preparation.

Immunofluorescence microscopic analysis

Cells grown on coverslips were fixed with ice-cold 4% paraformaldehyde in 100 mM phosphate buffer, pH 7.4, for 1 h on ice. The fixed cells were washed with 15 mM glycine in PBS (Gly-PBS) three times at 5-min intervals and then permeabilized with 0.1% Triton X-100 in Gly-PBS for 5 min at room temperature. After washing with Gly-PBS three times at 5-min intervals, the cells were incubated with 0.1% gelatin in PBS (gelatin-PBS) for 30 min at room temperature. The cells were then labeled with primary antibodies diluted in gelatin-PBS. After overnight reaction at 4°C, the cells were washed with gelatin-PBS three times at 5-min intervals and then incubated with secondary antibodies diluted in gelatin-PBS for 1 h at room temperature. After washing with gelatin-PBS three times at 5-min intervals and rinsing with PBS, the coverslips were mounted on microscopic slides. Fluorescence images were captured with an FV1000-D confocal laser-scanning microscope equipped with a ×60, 1.35 NA oil-immersion objective (UPLSAPO60XO; Olympus, Tokyo, Japan). Image analyses were carried out using IMAGE J (NIH, Bethesda, MD, USA).

Time-lapse imaging and FRAP analysis

For time-lapse imaging, HeLa cells transiently expressing GFP-TFG and mCherry-ALG-2 were grown on a glass-bottom dish (Asahi Glass, Tokyo, Japan). The medium was replaced with Leibovitz's L15 medium (Invitrogen) containing 1% fetal bovine serum. The cells were treated with 2 μM TG (DOJINDO, Kumamoto, Japan) or 1 mM dithiothreitol (Nacalai Tesque, Kyoto, Japan) diluted in the medium and then subjected to time-lapse imaging. Fluorescence intensities of GFP-TFG and mCherry-ALG-2 were measured using FV10-ASW software (Olympus). Based on the fluorescence intensity, $(F_t - F_0) / F_0$ ($\Delta F / F_0$) was calculated.

FRAP was performed as described previously [15, 23]. For quantitative analysis, independent normalized data from 16 cells expressing GFP-TFG^{WT} and GFP-$TFG^{\Delta ABM\text{-}2}$ were fitted globally to a one-phase exponential $F(t) = A_0 + A_1 (1 - e^{-kt})$, where A_0 is the offset of the curve, A_1 is the relative amplitude of the recovery curve, and k is the rate constant of fluorescence recovery corresponding to a dissociation rate from which $t_{1/2}$ values were determined, $t_{1/2} = \ln(2)/k$. These analyses were carried out using ORIGIN, version 9.1J (OriginLab Corp., Northampton, MA, USA). The relative sizes of the immobile and mobile

fractions were calculated as: immobile fraction = (1 - A_0 – A_1) / (1 – A_0); mobile fraction = A_1 / (1 – A_0).

Purification of recombinant proteins

TFG-His and its mutants were purified from Rosetta (DE3) pLysS carrying expression plasmids by using COSMOGEL His-Accept (Nacalai Tesque) in accordance with the manufacturer's instructions. N-terminal truncated ALG-2 (des3-20ALG-2) was purified as described previously [49].

***In vitro* binding assay and cross-linking assay using recombinant proteins**

For examination of oligomeric state of TFG-His, approximately 1 μM TFG-His was cross-linked by incubation with 0, 0.02, 0.05, 0.1, 0.2, 0.5, 1, 2 or 5 mM DTSSP (DOJINDO) in reaction buffer (20 mM Hepes-NaOH, pH 7.4, 142.5 mM KCl, 1.5 mM $MgCl_2$, 0.3% Chaps) at room temperature for 30 min. Cross-linking was quenched by incubation with 100 mM Tris-HCl (pH 8.0) at room temperature for 15 min. The products were prepared for SDS/PAGE by boiling at 95°C in Laemmli sample buffer (62.5 mM Tris-HCl, pH 6.8, 10% glycerol, 2% SDS, 0.002% bromophenol blue) supplemented with or without 5% 2-mercaptoethanol.

In *in vitro* binding assay of recombinant proteins, approximately 0.5 μM TFG-His was incubated with 0.5 μM des3-20ALG-2 in reaction buffer in the presence of 5 mM EGTA or 100 μM $CaCl_2$ at 4°C for 8 h. The reaction mixture was further incubated with anti-ALG-2 antibody at 4°C overnight. Then the mixture were incubated with Dynabeads Protein G at 4°C for 1 h. The beads were washed with reaction buffer containing 5 mM EGTA or 100 μM $CaCl_2$ twice and processed for sample preparation.

For examination of the effect of ALG-2, approximately 1 μM TFG-His was incubated with des3-20ALG-2 in the presence of 5 mM EGTA or 100 μM $CaCl_2$ at 4°C for 1 h and then cross-linked by incubation with 1 mM DTSSP for 30 min at room temperature. The subsequent manipulation was as described above.

siRNA-mediated RNAi interference

RNAi duplex oligoribonucleotides for TFG targeting 3'-UTR (siTFG: 5'-acaugauguacuaaaguagagccCT-3'; sequence of sense strand shown; deoxyribonucleotides indicated by uppercase letters), ALG-2 (siALG-2.1: 5'-agcaauaaagggaauguuagacgTG-3' and siALG-2.4: 5'-aaagacaggaguggagugauaucAG-3') and a negative control (siCtrl: 5'-cguuaaucgcguauaauacgcguAT-3') were purchased from Integrated DNA Technologies (Coralville, IA, USA). Cells were transfected with 10 nM siRNA duplexes targeting TFG, ALG-2 or negative control siRNA using Lipofectamine RNAiMAX (Invitrogen) in accordance with the forward transfection method and as described in the manufacturer's

instructions. Cells were analyzed 72 h after siRNA transfection.

Acknowledgement

We thank Satoshi Kamura for preparing recombinant des3-20ALG-2 proteins and all members of the Laboratory of Molecular and Cellular Regulation for their valuable suggestions and discussions. We also thank the late Professor Katsuko Tani and Assistant Professor Yuki Maemoto (Tokyo University of Pharmacy and Life Science) for providing antibodies against Sec16A and Sec16B. This work was supported in part by a Grant-in-Aid for Scientific Research (C) 15K07384 (to HS), a Grant-in-Aid for JSPS Fellows 14J09452 (to TK), a Grant-in-Aid for Scientific Research (B) 26292050 (to MM), a Grant-in-Aid for Young Scientists (B) 15K18680 (to TT) and a Grant-in-Aid for Scientific Research on Innovative Areas JP15H05955 (to KK). ITbM is supported by the World Premier International Research Center Initiative (WPI), Japan.

Author Contributions

TK planned and performed experiments, analyzed data and wrote the paper. KK performed the MS analysis. TT and MM advised on the experiments and data analysis. HS designed the study and wrote the paper.

References

1. Berridge MJ, Bootman MD & Roderick HL (2003) Calcium signalling: dynamics, homeostasis and remodeling. *Nat Rev Mol Cell Biol* **4**, 517-529.

2. Maki M, Narayana SV & Hitomi K (1997) A growing family of the Ca^{2+}-binding proteins with five EF-hand motifs. *Biochem J* **328**, 718-720.

3. Missotten M, Nichols A, Rieger K & Sadoul R (1999) Alix, a novel mouse protein undergoing calcium-dependent interaction with the apoptosis-linked-gene 2 (ALG-2) protein. *Cell Death Differ* **6**, 124–129.

4. Vito P, Pellegrini L, Guiet C & D'Adamio L (1999) Cloning of AIP1, a novel protein that associates with the apoptosis-linked gene ALG-2 in a Ca^{2+}-dependent reaction. *J Biol Chem* **274**, 1533–1540.

5. Katoh K, Suzuki H, Terasawa Y, Mizuno T, Yasuda J, Shibata H & Maki M (2005) The penta-EF-hand protein ALG-2 interacts directly with the ESCRT-I component TSG101, and Ca^{2+}-dependently co-localizes to aberrant endosomes with dominant-negative AAA ATPase SKD1/Vps4B. *Biochem J* **391**, 677-685.

6. Okumura M, Katsuyama AM, Shibata H & Maki M (2013) VPS37 isoforms differentially modulate the ternary complex formation of ALIX, ALG-2, and ESCRT-I. *Biosci Biotechnol Biochem* **77**, 1715–1721.

7. Satoh H, Nakano Y, Shibata H & Maki M (2002) The penta-EF-hand domain of ALG-2 interacts with amino-terminal domains of both annexin VII and annexin XI in a Ca^{2+}-dependent manner. *Biochim Biophys Acta* **1600**, 61–67.

8. Satoh H, Shibata H, Nakano Y, Kitaura Y & Maki M. (2002) ALG-2 interacts with the amino-terminal domain of annexin XI in a Ca^{2+}-dependent manner. *Biochem Biophys Res Commun* **291**, 1166–1172.

9. Shibata H, Suzuki H, Kakiuchi T, Inuzuka T, Yoshida H, Mizuno T & Maki M (2008) Identification of Alix-type and non-Alix-type ALG-2-binding sites in human phospholipid scramblase 3: differential binding to an alternatively spliced isoform and amino acid-substituted mutants. *J Biol Chem* **283**, 9623–9632.

10. Montaville P, Dai Y, Cheung CY, Giller K, Becker S, Michalak M, Webb SE, Miller AL & Krebs J (2006) Nuclear translocation of the calcium-binding protein ALG-2 induced by the RNA-binding protein RBM22. *Biochim Biophys Acta* **1763**, 1335-1343.

11. Yamasaki A, Tani K, Yamamoto A, Kitamura N & Komada, M (2006) The Ca^{2+}-binding protein ALG-2 is recruited to endoplasmic reticulum exit sites by Sec31A and stabilizes the localization of Sec31A. *Mol Biol Cell* **17**, 4876–4887.

12. Shibata H, Suzuki H, Yoshida H & Maki M (2007) ALG-2 directly binds Sec31A and localizes at endoplasmic reticulum exit sites in a Ca^{2+}-dependent manner. *Biochem Biophys Res Commun* **353**, 756–763.

13. Shibata H, Yamada K, Mizuno T, Yorikawa C, Takahashi H, Satoh H, Kitaura Y & Maki M (2004) The penta-EF-hand protein ALG-2 interacts with a region containing PxY repeats in Alix/AIP1, which is required for the subcellular punctate distribution of the amino-terminal truncation form of Alix/AIP1. *J Biochem* **135**, 117–128.

14. Trioulier Y, Torch S, Blot B, Cristina N, Chatellard-Causse C, Verna JM & Sadoul R (2004) Alix, a protein regulating endosomal trafficking, is involved in neuronal death. *J Biol Chem* **279**, 2046-2052.

15. Shibata H, Inuzuka T, Yoshida H, Sugiura H, Wada I & Maki M (2010) The ALG-2-binding site in Sec31A influences the retention kinetics of Sec31A at the endoplasmic reticulum exit sites as revealed by live-cell time-lapse imaging. *Biosci Biotechnol Biochem* **74**, 1819–1826.

16. Suzuki H, Kawasaki M, Inuzuka T, Okumura M, Kakiuchi T, Shibata H, Wakatsuki S & Maki M (2008) Structural basis for Ca^{2+}-dependent formation of ALG-2/Alix peptide complex: Ca^{2+} /EF3-driven arginine switch mechanism. *Structure* **16**, 1562–1573.

17. Takahashi T, Kojima K, Zhang W, Sasaki K, Ito M, Suzuki H, Kawasaki M, Wakatsuki S, Takahara T, Shibata H & Maki M (2015) Structural Analysis of the Complex between Penta-EF-Hand ALG-2 Protein and Sec31A Peptide Reveals a Novel Target Recognition Mechanism of ALG-2. *Int J Mol Sci* **16**, 3677-3699.

18. Osugi K, Suzuki H, Nomura T, Ariumi Y., Shibata H & Maki M (2012) Identification of the P-body component PATL1 as a novel ALG-2-interacting protein by *in silico* and far-Western screening of proline-rich proteins. *J Biochem* **151**, 657–666.

19. Sasaki-Osugi K, Imoto C, Takahara T, Shibata H & Maki M (2013) Nuclear ALG-2 protein interacts with Ca^{2+} homeostasis endoplasmic reticulum protein (CHERP) Ca^{2+}-dependently and participates in regulation of alternative splicing of inositol trisphosphate receptor type 1 (IP_3R1) pre-mRNA. *J Biol Chem* **288**, 33361–33375.

20. Lo KW, Zhang Q, Li M & Zhang M (1999) Apoptosis-linked gene product ALG-2 is a new member of the calpain small subunit subfamily of Ca^{2+}-binding proteins. *Biochemitry* **38**, 7498-7508.

21. Kitaura Y, Matsumoto S, Satoh H, Hitomi K & Maki M (2001) Peflin and ALG-2, members of the penta-EF-hand protein family, form a heterodimer that dissociates in a Ca^{2+}-dependent manner. *J Biol Chem* **276**, 14053–14058.

22. Okumura M, Ichioka F, Kobayashi R, Suzuki H, Yoshida H, Shibata H & Maki M (2009) Penta-EF-hand protein ALG-2 functions as a Ca-dependent adaptor that bridges Alix and TSG101. *Biochem Biophys Res Commun* **386**, 237–241.

23. Shibata H, Kanadome T, Sugiura H, Yokoyama T, Yamamuro M, Moss SE &Maki M (2015) A new role for annexin A11 in the early secretory pathway via stabilizing Sec31A protein at the endoplasmic reticulum exit sites (ERES). *J Biol Chem* **290**, 4981–4993.

24. Kitaura Y, Watanabe M, Satoh H, Kawai T, Hitomi K & Maki M (1999) Peflin, a novel member of the five-EF-hand-protein family, is similar to the apoptosis-linked gene 2 (ALG-2) protein but possesses nonapeptide repeats in the N-terminal hydrophobic region. *Biochem Biophys Res Commun* **263**, 68-75.

25. Greco A, Mariani C, Miranda C, Lupas A, Pagliardini S, Pomati M & Pierotti MA (1995) The DNA rearrangement that generates the TRK-T3 oncogene involves a novel gene on chromosome 3 whose product has a potential coiled-coil domain. *Mol Cell Biol* **15**, 6118-6127.

26. Witte K, Schuh AL, Hegermann J, Sarkeshik A, Mayers JR, Schwarze K, Yates JR 3rd, Eimer S &

Audhya A (2011) TFG-1 function in protein secretion and oncogenesis. *Nat Cell Biol* **13**, 550-558.

27. Johnson A, Bhattacharya N, Hanna M, Pennington JG, Schuh AL, Wang L, Otegui MS, Stagg SM & Audhya A (2015) TFG clusters COPII-coated transport carriers and promotes early secretory pathway organization. *EMBO J* **34**, 811-827.

28. Beetz C, Johnson A, Schuh AL, Thakur S, Varga RE, Fothergill T, Hertel N, Bomba-Warczak E, Thiele H, Nürnberg G, Altmüller J, Saxena R, Chapman ER, Dent EW, Nürnberg P & Audhya A (2013) Inhibition of TFG function causes hereditary axon degeneration by impairing endoplasmic reticulum structure. *Proc Natl Acad Sci USA* **110**, 5091-5096.

29. Ishiura H, Sako W, Yoshida M, Kawarai T, Tanabe O, Goto J, Takahashi Y, Date H, Mitsui J, Ahsan B, Ichikawa Y, Iwata A, Yoshino H, Izumi Y, Fujita K, Maeda K, Goto S, Koizumi H, Morigaki R, Ikemura M, Yamauchi N, Murayama S, Nicholson GA, Ito H, Sobue G, Nakagawa M, Kaji R & Tsuji S (2012) The TRK-fused gene is mutated in hereditary motor and sensory neuropathy with proximal dominant involvement. *Am J Hum Genet* **91**, 320-329.

30. la Cour JM, Mollerup J & Berchtold MW (2007) ALG-2 oscillates in subcellular localization, unitemporally with calcium oscillations. *Biochem Biophys Res Commun* **353**, 1063-1067.

31. Yoshida H, Haze K, Yanagi H, Yura T & Mori K (1998) Identification of the *cis*-acting endoplasmic reticulum stress response element responsible for transcriptional induction of mammalian glucose-regulated proteins; involvement of basic-leucine zipper transcription factors. *J Biol Chem* **273**, 33741–33749.

32. Haze K, Yoshida H, Yanagi H, Yura T & Mori K (1999) Mammalian transcription factor ATF6 is synthesized as a transmembrane protein and activated by proteolysis in response to endoplasmic reticulum stress. *Mol Biol Cell* **10**, 3787-3799.

33. la Cour JM, Schindler AJ, Berchtold MW & Schekman R (2013) ALG-2 attenuates COPII budding in vitro and stabilizes the Sec23/Sec31A complex. *PLoS One* **8**, e75309. doi: 10.1371/journal.pone.0075309.

34. Helm JR, Bentley M, Thorsen KD, Wang T, Foltz L, Oorschot V, Klumperman J & Hay JC (2014)

Apoptosis-linked gene-2 (ALG-2)/Sec31 interactions regulate endoplasmic reticulum (ER)-to-Golgi transport: a potential effector pathway for luminal calcium. *J Biol Chem* **289**, 23609-23628.

35. Maki M, Takahara T & Shibata H (2016) Multifaceted Roles of ALG-2 in Ca^{2+}-Regulated Membrane Trafficking. *Int J Mol Sci* **17**, 1401. doi: 10.3390/ijms17091401.

36. Yang X, Zou P, Yao J, Yun D, Bao H, Du R, Long J & Chen X (2010) Proteomic dissection of cell type-specific H2AX-interacting protein complex associated with hepatocellular carcinoma. *J Proteome Res* **9**, 1402-1415.

37. Wiemuth D, van de Sandt L, Herr R & Gründer S (2012) Transient receptor potential N (TRPN1) from *Xenopus* interacts with the penta-EF-hand protein peflin. *FEBS Lett* **586**, 4276-4281.

38. Rayl M, Truitt M, Held A, Sargeant J, Thorsen K & Hay JC (2016) Penta-EF-Hand Protein Peflin Is a Negative Regulator of ER-To-Golgi Transport. *PLoS One* **11**, e0157227. doi: 10.1371/journal.pone.0157227.

39. Takahashi T, Suzuki H, Inuzuka T, Shibata H & Maki M (2012) Prediction of a new ligand-binding site for type 2 motif based on the crystal structure of ALG-2 by dry and wet approaches. *Int J Mol Sci* **13**, 7532-7549.

40. Maki M, Suzuki H & Shibata H (2011) Structure and function of ALG-2, a penta-EF-hand calcium-dependent adaptor protein. *Sci China Life Sci* **54**, 770-779.

41. Hay JC (2007) Calcium: a fundamental regulator of intracellular membrane fusion? *EMBO Rep* **8**, 236-240.

42. Bentley M, Nycz DC, Joglekar A, Fertschai I, Malli R, Graier WF & Hay JC (2010) Vesicular calcium regulates coat retention, fusogenicity, and size of pre-Golgi intermediates. *Mol Biol Cell* **21**, 1033-1046.

43. la Cour JM, Mollerup J, Winding P, Tarabykina S, Sehested M & Berchtold MW (2003) Up-regulation of ALG-2 in hepatomas and lung cancer tissue. *Am J Pathol* **163**, 81-89.

44. la Cour JM, Høj BR, Mollerup J, Simon R, Sauter G & Berchtold MW (2008) The apoptosis linked gene ALG-2 is dysregulated in tumors of various origin and contributes to cancer cell viability. *Mol Oncol* **1**, 431-439.

45. Greco A, Fusetti L, Miranda C, Villa R, Zanotti S, Pagliardini S & Pierotti MA (1998) Role of the TFG N-terminus and coiled-coil domain in the transforming activity of the thyroid TRK-T3 oncogene. *Oncogene* **16**, 809-816.

46. Iinuma T, Shiga A, Nakamoto K, O'Brien MB, Aridor M, Arimitsu N, Tagaya M & Tani K (2007) Mammalian Sec16/p250 plays a role in membrane traffic from the endoplasmic reticulum. *J Biol Chem* **282**, 17632-17639.

47. Yonekawa S, Furuno A, Baba T, Fujiki Y, Ogasawara Y, Yamamoto A, Tagaya M & Tani K (2011) Sec16B is involved in the endoplasmic reticulum export of the peroxisomal membrane biogenesis factor peroxin 16 (Pex16) in mammalian cells. *Proc Natl Acad Sci USA* **108**, 12746-112751.

48. McCaughey J, Miller VJ, Stevenson NL, Brown AK, Budnik A, Heesom KJ, Alibhai D & Stephens DJ (2016) TFG Promotes Organization of Transitional ER and Efficient Collagen Secretion. *Cell Rep* **15**, 1648-1659.

49. Inuzuka T, Suzuki H, Kawasaki M, Shibata H, Wakatsuki S & Maki M (2010) Molecular basis for defect in Alix-binding by alternatively spliced isoform of ALG-2 (ALG-2$^{\Delta GF122}$) and structural roles of F122 in target recognition. *BMC Struct Biol* **10**, 25. doi: 10.1186/1472-6807-10-25.

50. Ueda H, Yokota E, Kuwata K, Kutsuna N, Mano S, Shimada T, Tamura K, Stefano G, Fukao Y, Brandizzi F, Shimmen T, Nishimura M & Hara-Nishimura I (2016) Phosphorylation of the C Terminus of RHD3 Has a Critical Role in Homotypic ER Membrane Fusion in Arabidopsis. *Plant Physiol* **170**, 867-880.

Supporting Information

Table S1. A list of the identified peptides and corresponding proteins by LC-MS/MS analysis

Table 1. Relative rates of immobile and mobile fractions, and half-lives ($t_{1/2}$) of WT and ΔABM-2

Values are the means ± SEM. ***P* < 0.01

GFP-TFG	Immobile	Mobile	$t_{1/2}$ (sec)
WT	0.149 ± 0.015	0.851 ± 0.015	1.82 ± 0.17
ΔABM-2	0.077 ± 0.011**	0.923 ± 0.011**	1.21 ± 0.10**

Figure legends

Fig. 1. ALG-2 binds to TFG in a Ca^{2+}-dependent manner. (A) Cleared cell lysates from HEK293/ALG-2_{KD} cells co-expressing FLAG-ALG-$2^{E47A/E114A}$ and either ALG-2 or peflin were incubated with anti-FLAG antibody and protein G-conjugated magnetic beads in the presence of 10 μM $CaCl_2$. Bound proteins were eluted by incubation of the beads with 5 mM EGTA. The eluates (EGTA elution) and beads remaining after EGTA elution (Beads) were analyzed by SDS/PAGE followed by silver staining. The indicated bands (a1-a4) were excised and analyzed by LC-MS/MS. (B, C) Cleared cell lysates from HEK293 cells were incubated with the indicated antibodies and protein G-conjugated magnetic beads in the presence of 5 mM EGTA or 100 μM $CaCl_2$. Cleared cell lysate proteins (Input) and bound proteins (IP) were analyzed by SDS/PAGE followed by western blotting using the indicated antibodies. The relative amounts of cleared cell lysate proteins (Input) used for analysis of immunoprecipitation products (IP) were 0.5% (B, upper) and 2.5% (B, lower, and C).

Fig. 2. GST-pulldown assays of ALG-2 and TFG mutants. (A) Glutathione-sepharose beads containing GST (Ctrl), wild-type GST-ALG-2 (WT) or GST-ALG-2 mutants (Y180A and F85A) were incubated with cleared cell lysates from HEK293/ALG-2_{KD} cells in the presence of 10 μM $CaCl_2$. Cleared lysate (Input) and pulldown products (Pulldown) were subjected to SDS/PAGE (12% for anti-TFG antibody) followed by western blotting using the indicated antibodies. The relative amount of cleared lysate (Input) used for analysis of pulldown products (Pulldown) was 2.5% (B) Schematic diagrams of GFP-fused TFG and its mutants. CC, coiled-coil. (C-E) Glutathione-sepharose beads containing wild-type GST-ALG-2 were incubated with cleared cell lysates from HEK293 cells expressing GFP (Ctrl), wild-type GFP-TFG (WT) or GFP-TFG mutants [ΔABM-2 (C); ΔPB1, ΔCC, ΔCt, ΔNt (D); R106C, P285L (E)] in the presence of 10 μM $CaCl_2$. Cleared lysate (Input) and pulldown products (Pulldown) were subjected to SDS/PAGE followed by western blotting using the indicated antibodies. The relative amount of cleared lysate (Input) used for analysis of pulldown products (Pulldown) was 5%.

Fig. 3. ALG-2 partially co-localizes with TFG at Sec31A-positive ERES. HeLa cells were subjected to co-immunostaining using anti-TFG antibody (A, D), anti-ALG-2 antibody (B, E) and anti-Sec31A antibody (C, F). Parts (D), (E) and (F) are magnified views of the area within a white square, as indicated in (C), in (A), (B) and (C), respectively. Merged images with pseudocolors are shown (G-J). Arrows and arrowheads in (G-J) indicate TFG-positive puncta overlapping and not overlapping with ALG-2/Sec31A-positive structures, respectively. Scale bars = 20 μm in (C) and 5 μm in (F).

Fig. 4. TFG and Sec31A are not bridged by ALG-2. Cleared cell lysates from HEK293 cells co-expressing FLAG-ALG-2 and GFP or GFP-TFG were incubated with anti-GFP antibody and protein G-conjugated magnetic beads in the presence of 5 mM EGTA or 10 μM $CaCl_2$. Cleared lysate (Input) and bound proteins (IP) were analyzed by SDS/PAGE followed by western blotting using the indicated antibodies. The relative amounts of cleared lysate (Input) used for analysis of immunoprecipitation products (IP) were 2.5% (upper and middle) and 10% (lower).

Fig. 5. TFG and ALG-2 are concentrated to ERES upon treatment with TG. (A) GFP-fused TFG (GFP-TFG) and mCherry-fused ALG-2 (mCherry-ALG-2) were transiently co-expressed in HeLa cells. Time-lapse images before (B, time 0 sec) and after (B, time 50–300 s) administration of 2 μM TG were acquired using a confocal microscope. Scale bar = 20 μm. (B) Representative sequential time-lapse images of GFP-TFG and mCherry-ALG-2 in the area of the white square as indicated in (A) were extracted and are shown. Scale bar = 5 μm. (C) The fluorescence intensities of the region indicated by a white circle in (B) were quantified, and changes in relative fluorescence intensity ($\Delta F/F_0$) of GFP-TFG and mCherry-ALG-2 were plotted over time. (D, E) The fluorescence intensities of regions including a double positive puncta for GFP-TFG and mCherry ALG-2 were measured before (Pre, time 0 s in B) and after (Post, time 150 s in B) administration of 2 μM TG (D) or 1 mM dithiothreitol (DTT) (E). Values and bars represent mean ± SEM fluorescence intensity (arbitrary units) (D: n = 27 from seven independent experiments; E: n = 21 from six independent experiments). Statistical significance of differences was analyzed by a paired Student's t test. Asterisks indicate a statistically significant difference (***P < 0.001).

Fig. 6. Overexpression of ALG-2 leads to accumulation of TFG in cytoplasmic punctate structures. (A, B) HeLa cells transfected with the expression plasmid for FLAG-ALG-2^{WT} or FLAG-ALG-$2^{E47A/E114A}$ were subject to co-immunostaining using anti-FLAG antibody and anti-TFG antibody (A) or anti-Sec31A antibody (B). Transfected cells and untransfected cells are indicated by plus signs (+) and minus signs (-), respectively (left). Scale bars = 20 μm. The mean of fluorescence intensity of TFG-positive puncta (A) or Sec31A-positive puncta (B) per cell was quantified (right). Error bars represent the means ± SEM. (A) Transfection with expression plasmid for FLAG-ALG-2^{WT} (n = 21, untransfected cells; n = 21, transfected cells) and transfection with expression plasmid for FLAG-ALG-$2^{E47A/E114A}$ (n = 17, untransfected cells; n = 22, transfected cells). ***P < 0.001; (B) Transfection with expression plasmid for FLAG-ALG-2^{WT} (n = 18, untransfected cells; n = 12, transfected cells) and transfection with expression plasmid for FLAG-ALG-$2^{E47A/E114A}$ (n = 17, untransfected cells; n = 11, transfected cells). (C) HeLa cells transfected with an empty vector (Ctrl), FLAG-ALG-2^{WT} (WT) or FLAG-ALG-$2^{E47A/E114A}$ (E47A/E114A) constructs were

subject to SDS/PAGE followed by western blotting using the indicated antibodies (left). Although the western blot with anti-FLAG antibody shows that both FLAG-ALG-2^{WT} and FLAG-ALG-2$^{E47A/E114A}$ are expressed in transfected HeLa cells (Blot: anti-FLAG), a weak signal for FLAG-ALG-2$^{E47A/E114A}$ was detected in the western blot with a rabbit polyclonal antibody against ALG-2 (Blot: anti-ALG-2), suggesting reduced reactivity of the antibody to the mutant. HeLa cells treated with (TG) or without (DMSO) TG (100 nM) for 16 h were subject to SDS/PAGE followed by western blotting using the indicated antibodies (right). (D) Cleared cell lysates from HEK293/ALG-2$_{KD}$ cells transfected with the expression plasmid for FLAG-ALG-2^{WT} or FLAG-ALG-2$^{E47A/E114A}$ were incubated with anti-FLAG antibody and protein G-conjugated magnetic beads in the presence of 10 μM $CaCl_2$. Cleared lysate (Input) and bound proteins (IP) were analyzed by SDS/PAGE and western blotting using the indicated antibodies. The relative amounts of cleared lysate (Input) used for analysis of immunoprecipitation products (IP) were 2.5% (upper and middle) and 10% (lower). (E) HeLa cells transfected with control (siCtrl) or ALG-2 (siALG-2.1 or siALG-2.4) siRNAs were subject to co-immunostaining using anti-TFG antibody and anti-ALG-2 antibody. Scale bars = 20 μm. The mean of fluorescence intensity of TFG-positive puncta per cell was quantified (right). Error bars represent the means ± SEM. Transfection with siRNAs for control (siCtrl, n = 19) and ALG-2 (siALG-2.1, n = 19 and siALG-2.4, n = 20). The statistical significance of differences was analyzed by one-way ANOVA, followed by Tukey's test (siCtrl vs siALG-2.1, P = 0.309; siCtrl vs siALG-2.4, P = 0.908); n.s., not significant.

Fig. 7. GFP-TFG mutant lacking an ALG-2-binding motif has an impairment in the stable retention at ERES. (A) HeLa cells expressing wild-type GFP-TFG (WT) or ABM-2-deleted GFP-TFG (ΔABM-2) were subject to immunostaining using anti-Sec31A antibody. Lower left insets: magnified views of the white squares as indicated in the merged images. Scale bars = 20 μm. (B) HeLa cells expressing wild-type GFP-TFG were subject to immunostaining using anti-ALG-2 antibody. Lower: magnified views of white square as indicated to the upper right. Scale bars = 20 μm (upper) and 5 μm (lower). (C) Representative FRAP experiment using HeLa cells expressing GFP fusion proteins. GFP-positive dots were photobleached and fluorescence recovery was followed (left) and plotted over time (right). Scale bars = 1 μm. (D) Quantitative FRAP analysis of GFP-TFG (WT) and GFP-TFG$^{\Delta ABM-2}$ (ΔABM-2). Normalized mean recovery rate after photobleaching for WT (black, n = 16) and ΔABM-2 (red, n = 16) is plotted. Error bars represent 95% confidence intervals.

Fig. 8. TFG forms oligomers *in vitro*. Recombinant TFG-His proteins were incubated with the indicated concentration of DTSSP for 30 min at room temperature. The reaction was terminated by adding 100 mM

Tris-HCl (pH 8.0). The products were processed for SDS/PAGE without (upper) or with (lower) 2-mercaptoethanol and analyzed by SDS/PAGE and western blotting using anti-TFG antibody. Filled and open arrowheads in lower panel indicate unmodified and modified forms of TFG, respectively.

Fig. 9. ALG-2 promotes polymerization of TFG in a Ca^{2+}-dependent manner *in vitro*. (A) Recombinant TFG-His proteins (0.5 μM) were incubated with or without des3-20ALG-2 (0.5 μM) in the presence of 5 mM EGTA or 100 μM $CaCl_2$ (Input). Then, the mixtures were immunoprecipitated with anti-ALG-2 antibody (IP). Input and IP fractions were analyzed by SDS/PAGE and western blotting using indicated antibodies. The relative amount of Input fractions used for analysis of IP products was 2.5%. (B, C) TFG-His was incubated with the indicated concentration of des3-20ALG-2 in the presence of 5 mM EGTA or 100 μM $CaCl_2$ for 1 h at 4ºC and then cross-linked by incubation with 1 mM DTSSP for 30 min at room temperature. The reaction was terminated by adding 100 mM Tris-HCl (pH 8.0). The products were processed for SDS/PAGE without (upper) or with (lower) 2-mercaptoethanol and analyzed by SDS/PAGE and western blotting using anti-TFG antibody (B) and anti-ALG-2 antibody (C). (D) des3-20ALG-2 proteins without TFG-His were cross-linked by DTSSP and analyzed as described above. Arrows represent the positions at the wells of the gel.

Fig. 10. TFG mutant lacking an ALG-2-binding motif has an impairment in its polymerization by ALG-2. (A, B) TFG-His mutants, ΔABM-2 (A) and R106C (B), were subjected to a cross-linking assay as described in Fig. 8. Filled and open arrowheads in lower panels indicate unmodified and modified forms of the recombinant proteins, respectively. (C, D) TFG-His (WT) and its mutants (ΔABM-2 and R106C) were incubated with indicated concentrations of des3-20ALG-2 in the presence of 100 μM $CaCl_2$ and subjected to the cross-linking assay as described in the legend of Fig. 9. Arrows represent the positions at the wells of the gel. (D) Bands of the TFG-His oligomer entering the gel in (C, upper left) were quantified and plotted as relative intensity to that of each oligomer without des3-20ALG-2. Error bars represents the means ± SEM (n = 3). The statistical significance of differences was analyzed by one-way ANOVA followed by Tukey's test. *P < 0.05, **P < 0.01.

Fig. 1.

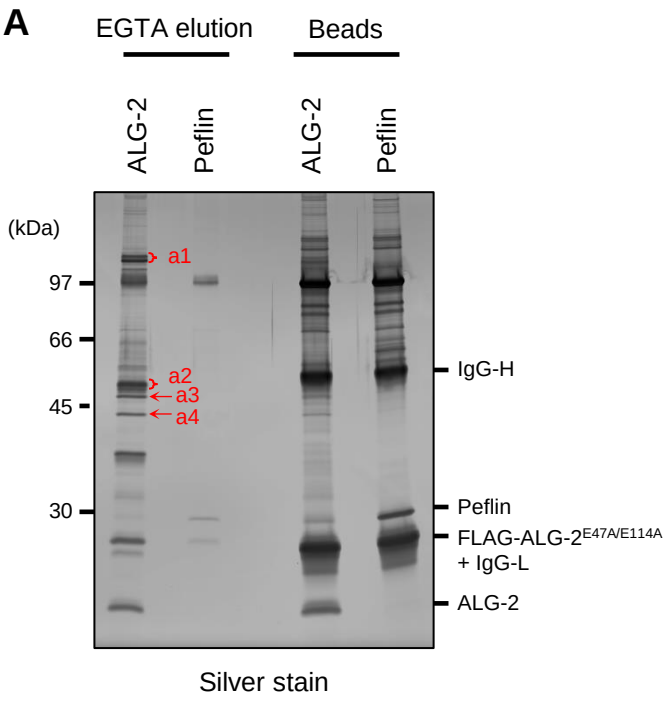
A
EGTA elution
Beads
ALG-2
Peflin
ALG-2
Peflin
(kDa)
97
66
45
30
a1
a2
a3
a4
IgG-H
Peflin
FLAG-ALG-2E47A/E114A
+ IgG-L
ALG-2
Silver stain

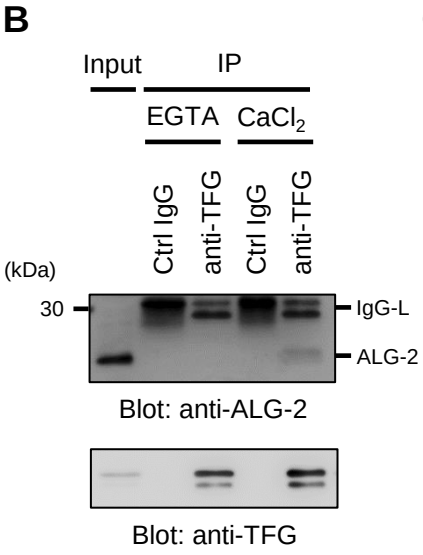
B
Input
IP
EGTA
CaCl2
Ctrl IgG
anti-TFG
Ctrl IgG
anti-TFG
(kDa)
30
IgG-L
ALG-2
Blot: anti-ALG-2
Blot: anti-TFG

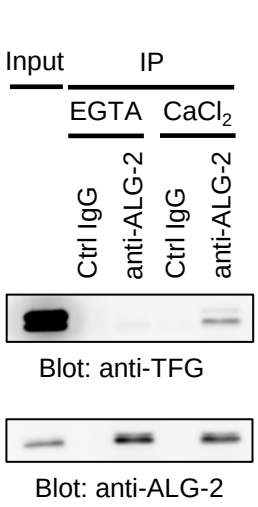
C
Input
IP
EGTA
CaCl2
Ctrl IgG
anti-ALG-2
Ctrl IgG
anti-ALG-2
Blot: anti-TFG
Blot: anti-ALG-2

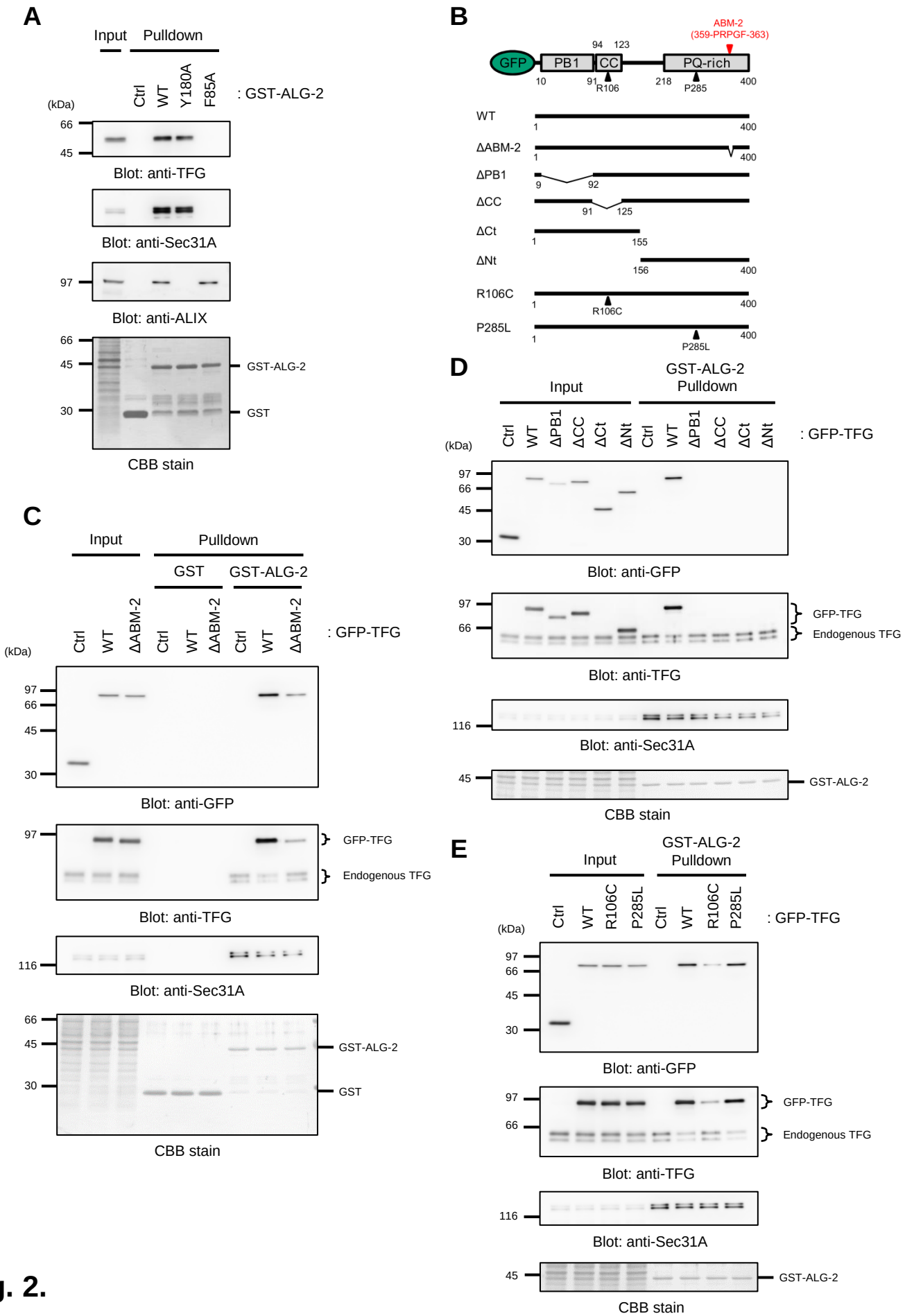
A
Input
Pulldown
Ctrl
WT
Y180A
F85A
: GST-ALG-2
(kDa)
66
45
Blot: anti-TFG
Blot: anti-Sec31A
97
Blot: anti-ALIX
GST-ALG-2
30
GST
CBB stain
B
ABM-2
(359-PRPGF-363)
94
123
GFP
PB1
CC
PQ-rich
10
91
R106
218
P285
400
WT
ΔABM-2
ΔPB1
9
92
ΔCC
125
ΔCt
155
ΔNt
156
R106C
P285L
C
GST
GST-ALG-2
ΔABM-2
: GFP-TFG
Blot: anti-GFP
GFP-TFG
Endogenous TFG
Blot: anti-TFG
116
Blot: anti-Sec31A
CBB stain
D
ΔPB1
ΔCC
ΔCt
ΔNt
Blot: anti-GFP
Blot: anti-TFG
Blot: anti-Sec31A
CBB stain
E
R106C
P285L
Blot: anti-GFP
Blot: anti-TFG
Blot: anti-Sec31A
CBB stain

Fig. 2.

Fig. 3.

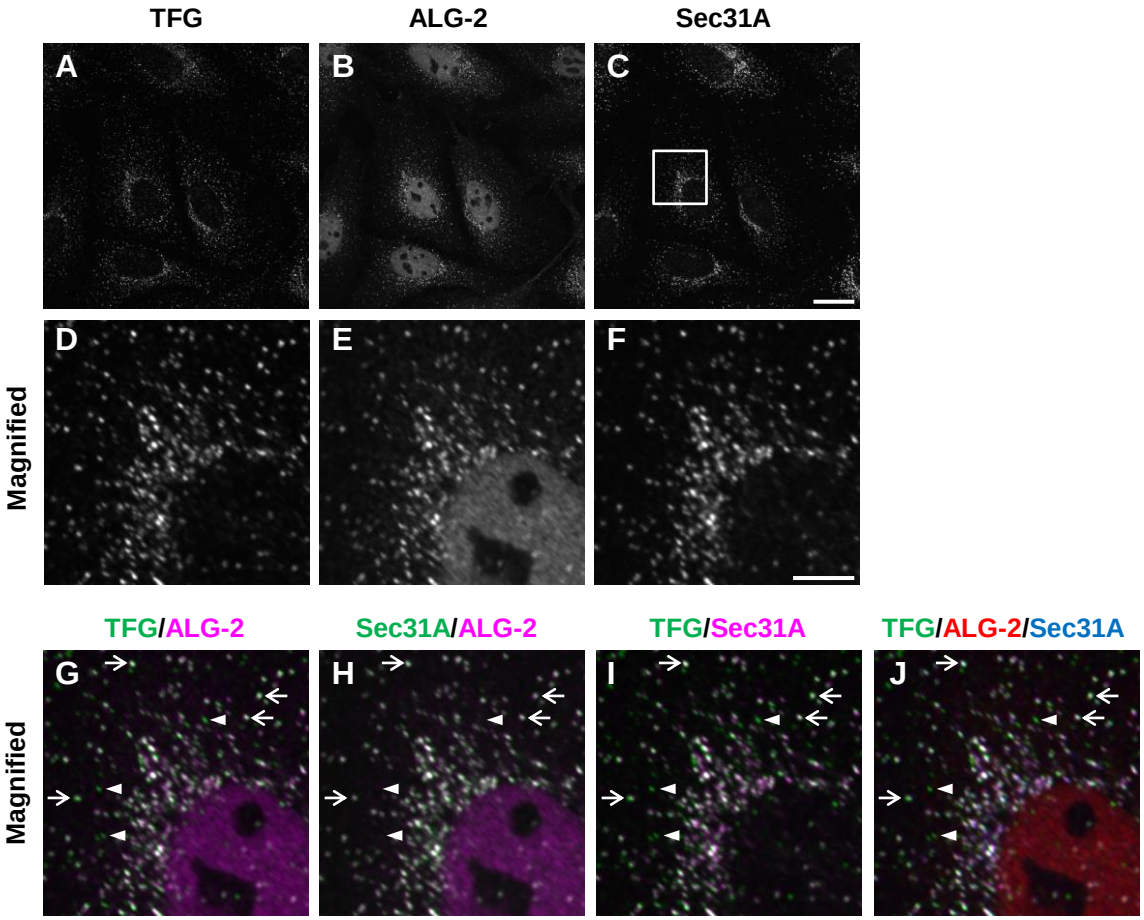
TFG
ALG-2
Sec31A
A
B
C
D
E
F
Magnified
TFG/ALG-2
Sec31A/ALG-2
TFG/Sec31A
TFG/ALG-2/Sec31A
G
H
I
J
Magnified

Fig. 4.

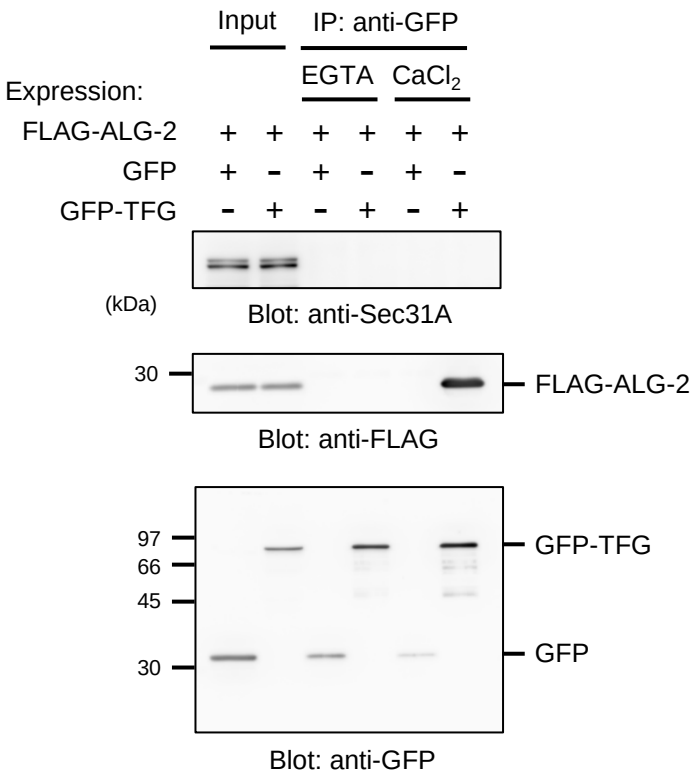
Input
IP: anti-GFP
EGTA
CaCl2
Expression:
FLAG-ALG-2 + + + + + +
GFP + - + - + -
GFP-TFG - + - + - +
(kDa)
Blot: anti-Sec31A
30
FLAG-ALG-2
Blot: anti-FLAG
97
66
45
30
GFP-TFG
GFP
Blot: anti-GFP

Fig. 5.

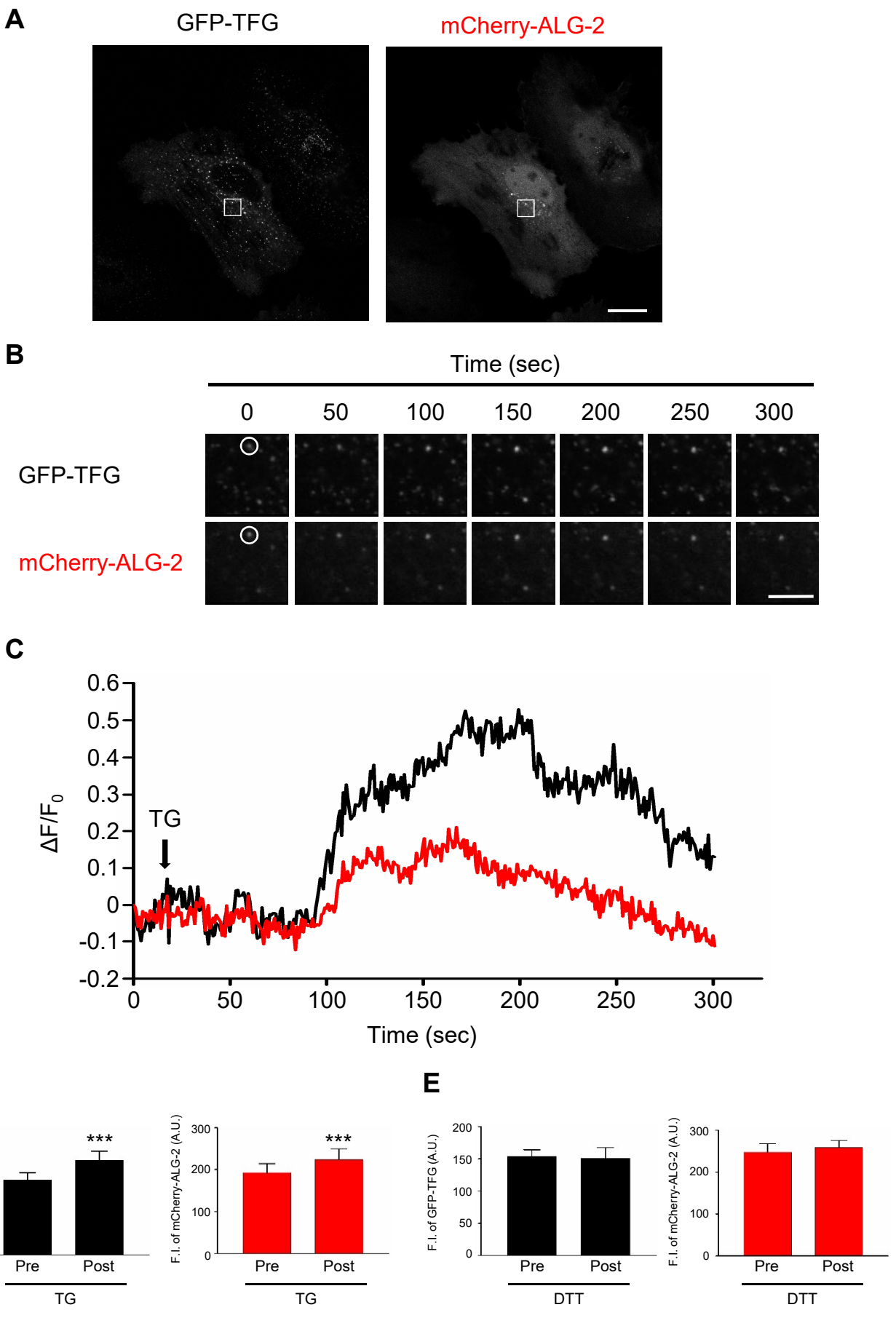
A
GFP-TFG
mCherry-ALG-2
B
Time (sec)
0
50
100
150
200
250
300
GFP-TFG
mCherry-ALG-2
C
ΔF/F0
TG
Time (sec)
D
F.I. of GFP-TFG (A.U.)
F.I. of mCherry-ALG-2 (A.U.)
***
Pre
Post
TG
E
DTT

Fig. 6.

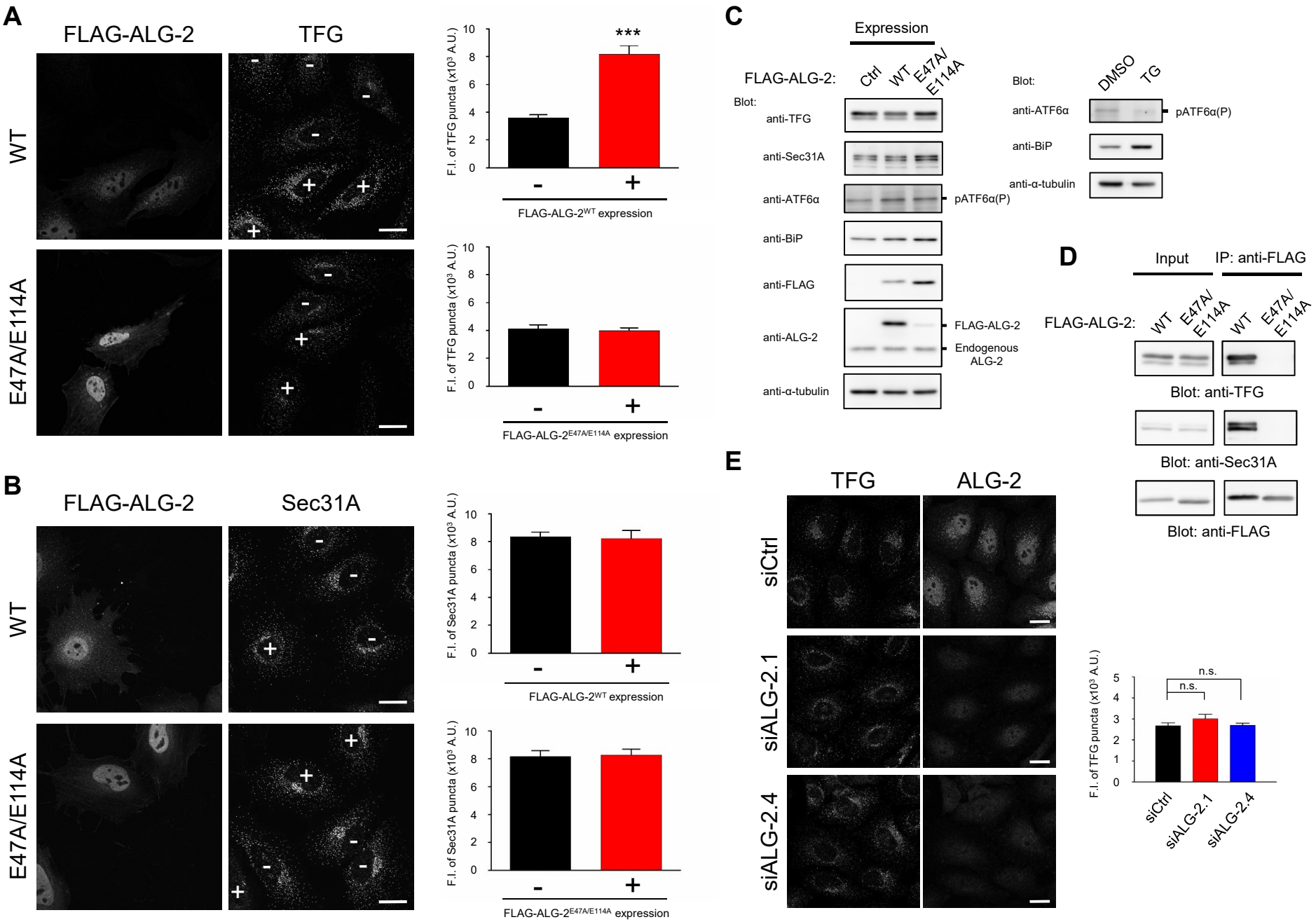
A
FLAG-ALG-2
TFG
WT
E47A/E114A
F.I. of TFG puncta (x10³ A.U.)
***
FLAG-ALG-2WT expression
FLAG-ALG-2E47A/E114A expression
B
FLAG-ALG-2
Sec31A
F.I. of Sec31A puncta (x10³ A.U.)
C
Expression
FLAG-ALG-2:
Ctrl
WT
E47A/E114A
Blot:
anti-TFG
anti-Sec31A
anti-ATF6α
pATF6α(P)
anti-BiP
anti-FLAG
anti-ALG-2
FLAG-ALG-2
Endogenous ALG-2
anti-α-tubulin
DMSO
TG
D
Input
IP: anti-FLAG
Blot: anti-TFG
Blot: anti-Sec31A
Blot: anti-FLAG
E
TFG
ALG-2
siCtrl
siALG-2.1
siALG-2.4
n.s.
siCtrl
siALG-2.1
siALG-2.4

Fig. 7.

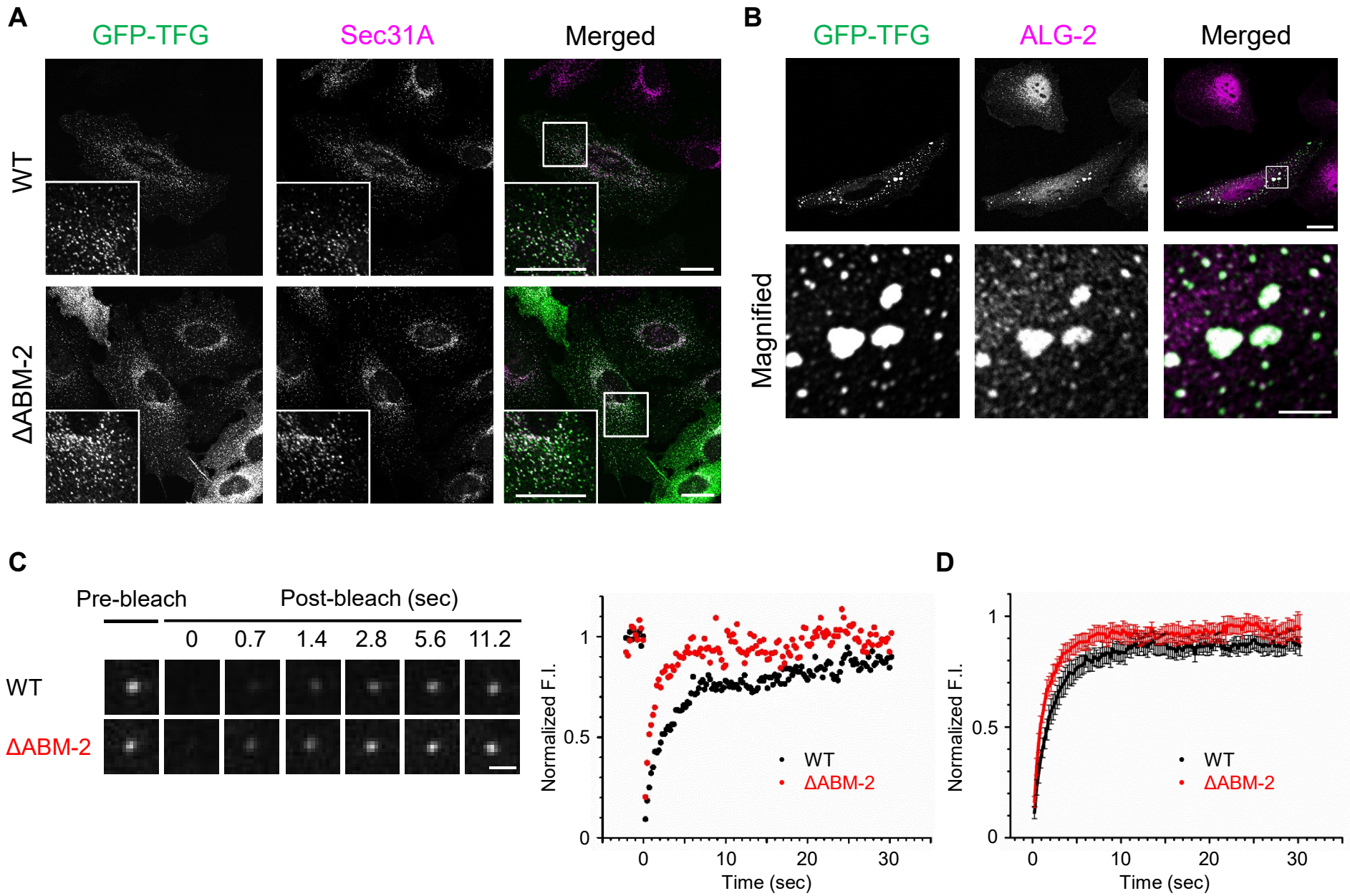
A
GFP-TFG
Sec31A
Merged
WT
ΔABM-2
B
GFP-TFG
ALG-2
Merged
Magnified
C
Pre-bleach
Post-bleach (sec)
0
0.7
1.4
2.8
5.6
11.2
WT
ΔABM-2
Normalized F.I.
Time (sec)
WT
ΔABM-2
D
Normalized F.I.
Time (sec)
WT
ΔABM-2

Fig. 8.

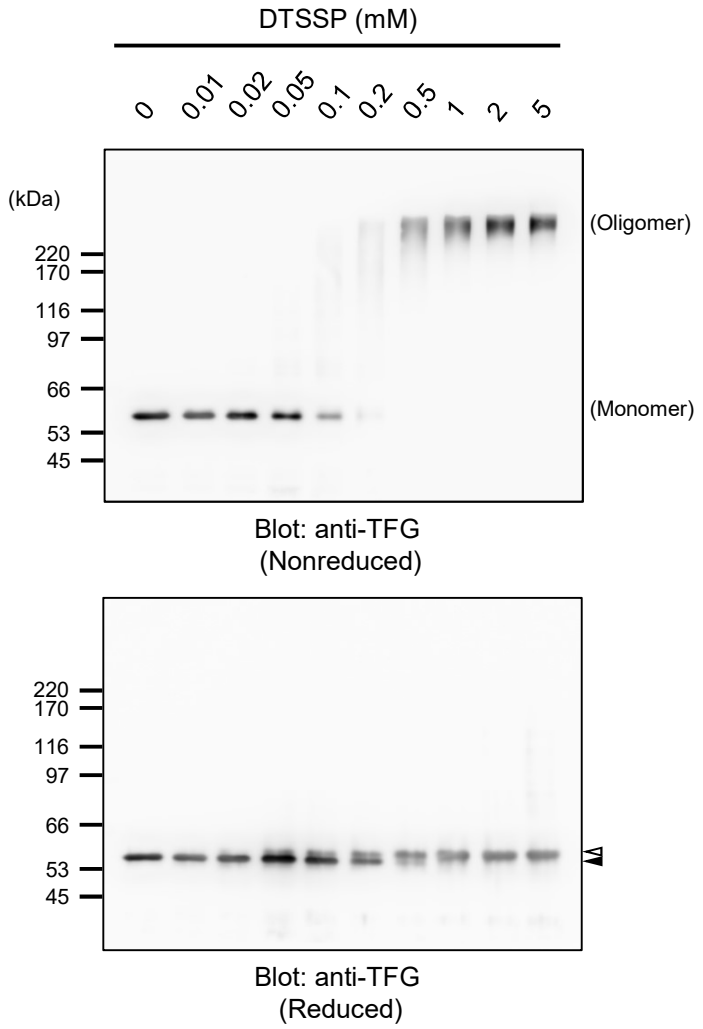
DTSSP (mM)
0
0.01
0.02
0.05
0.1
0.2
0.5
1
2
5
(kDa)
220
170
116
97
66
53
45
(Oligomer)
(Monomer)
Blot: anti-TFG
(Nonreduced)
220
170
116
97
66
53
45
Blot: anti-TFG
(Reduced)

Fig. 9.

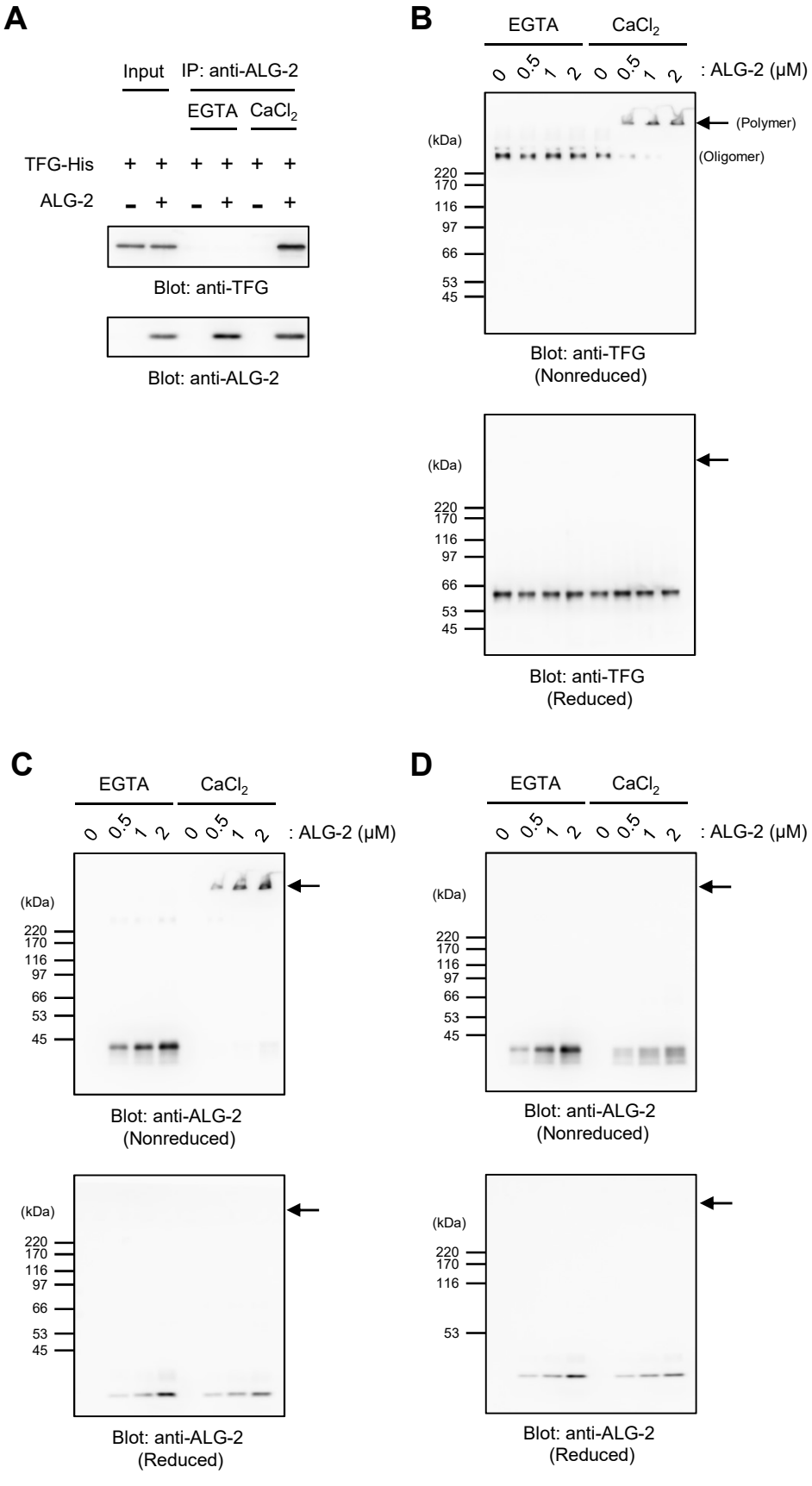
A
Input
IP: anti-ALG-2
EGTA
CaCl2
TFG-His
ALG-2
Blot: anti-TFG
Blot: anti-ALG-2
B
EGTA
CaCl2
0 0.5 1 2 0 0.5 1 2 : ALG-2 (μM)
(kDa)
(Polymer)
(Oligomer)
220
170
116
97
66
53
45
Blot: anti-TFG
(Nonreduced)
Blot: anti-TFG
(Reduced)
C
EGTA
CaCl2
0 0.5 1 2 0 0.5 1 2 : ALG-2 (μM)
(kDa)
220
170
116
97
66
53
45
Blot: anti-ALG-2
(Nonreduced)
Blot: anti-ALG-2
(Reduced)
D
EGTA
CaCl2
0 0.5 1 2 0 0.5 1 2 : ALG-2 (μM)
(kDa)
220
170
116
97
66
53
45
Blot: anti-ALG-2
(Nonreduced)
Blot: anti-ALG-2
(Reduced)

Fig. 10.

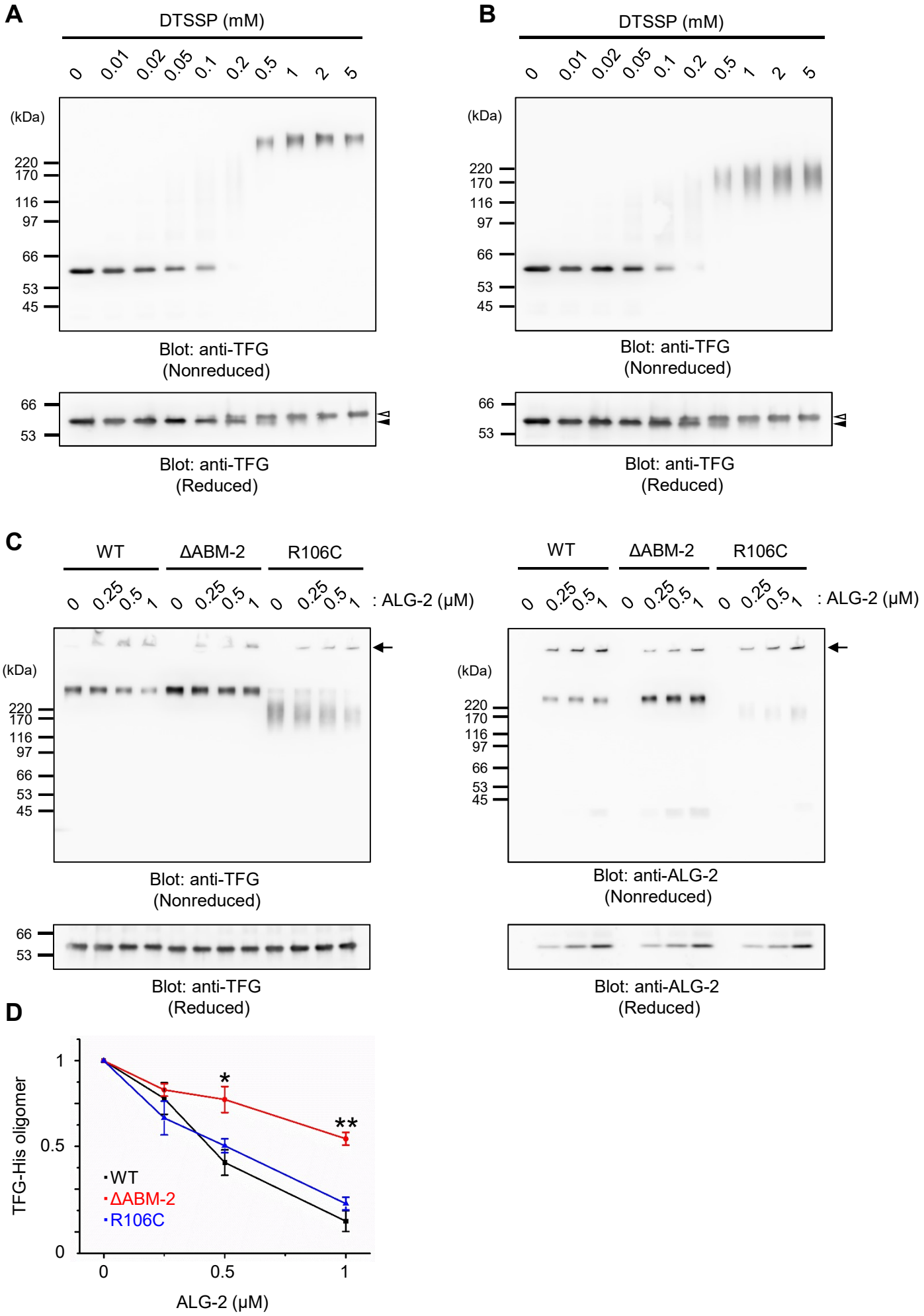
A
DTSSP (mM)
0 0.01 0.02 0.05 0.1 0.2 0.5 1 2 5
(kDa)
220
170
116
97
66
53
45
Blot: anti-TFG
(Nonreduced)
66
53
Blot: anti-TFG
(Reduced)
B
DTSSP (mM)
0 0.01 0.02 0.05 0.1 0.2 0.5 1 2 5
(kDa)
220
170
116
97
66
53
45
Blot: anti-TFG
(Nonreduced)
66
53
Blot: anti-TFG
(Reduced)
C
WT
ΔABM-2
R106C
0 0.25 0.5 1 0 0.25 0.5 1 0 0.25 0.5 1 : ALG-2 (μM)
(kDa)
220
170
116
97
66
53
45
Blot: anti-TFG
(Nonreduced)
66
53
Blot: anti-TFG
(Reduced)
WT
ΔABM-2
R106C
0 0.25 0.5 1 0 0.25 0.5 1 0 0.25 0.5 1 : ALG-2 (μM)
(kDa)
220
170
116
97
66
53
45
Blot: anti-ALG-2
(Nonreduced)
Blot: anti-ALG-2
(Reduced)
D
TFG-His oligomer
1
0.5
0
0
0.5
1
ALG-2 (μM)
*
**
WT
ΔABM-2
R106C

Table S1. A list of the identified peptides and corresponding proteins by LC-MS/MS analysis

Digested bands	Protein name	Number of peptides	Sequences of identified peptides
a1	Sec31A	53	59-SCATFSSSHR-68
			72-LIWGPYK-78
			106-IIAGDKEVVIAQNDK-120
			112-EVVIAQNDK-120
			112-EVVIAQNDKHTGPVR-126
			165-TQPPEDISCIAWNR-178
			179-QVQHILASASPSGR-192
			193-ATVWDLR-199
			200-KNEPIIK-206
			201-NEPIIKVSDHSNR-213
			207-VSDHSNR-213
			255-VLENHAR-261
			315-NPAVLSAASFDGR-327
			328-ISVYSIMGGSTDGLR-342
			328-ISVYSIMGGSTDGLRQK-344
			392-RPVGASFSFGGK-403
			404-LVTFENVR-411
			412-MPSHQGAEQQQQQHHVFISQVVTEK-436
			442-SDQLQQAVQSQGFINYCQK-460
			461-KIDASQTEFEK-471
			462-IDASQTEFEK-471
			472-NVWSFLK-478
			479-VNFEDDSR-486
			479-VNFEDDSRGK-488
			489-YLELLGYR-496
			489-YLELLGYRK-497
			489-YLELLGYRKEDLGK-502
			497-KEDLGKK-503
			503-KIALALNK-510
			504-IALALNKVDGANVALK-519
			628-LITAVVMK-635
			708-AQDGSHPLSLQDLIEK-723
			729-KAVQLTQAMDTSTVGVLLAAK-749
			730-AVQLTQAMDTSTVGVLLAAK-749
			789-AQGEPVAGHESPK-801
			789-AQGEPVAGHESPKIPYEK-806
			802-IPYEKQQLPK-811
			812-GRPGPVAGHHQMPR-823
			989-TGPQNGWNDPPALNR-1003
			989-TGPQNGWNDPPALNRVPK-1006
			1107-ITKKPIPDEHLILK-1120
			1110-KPIPDEHLILK-1120
			1121-TTFEDLIQR-1129
			1130-CLSSATDPQTK-1140
			1130-CLSSATDPQTKR-1141
			1143-LDDASKR-1149
			1149-RLEFLYDK-1156
			1149-RLEFLYDKLR-1158
			1150-LEFLYDK-1156
			1157-LREQTLSPTITSGLHNIAR-1175
			1159-EQTLSPTITSGLHNIAR-1175
			1210-VVLTQANK-1217
			1210-VVLTQANKLGV-1220
a2	TFG	10	15-AQLGEDIR-22
			15-AQLGEDIRR-23
			48-LLSNDEVTIK-57
			86-LTLFVNGQPRPLESSQVK-103
			119-LLDSLEPPGEPGPSTNIPENDTVDGR-144
			119-LLDSLEPPGEPGPSTNIPENDTVDGREEK-147
			156-QSTQVMAASMSAFDPLK-172
			156-QSTQVMAASMSAFDPLKNQDEINK-179
			180-NVMSAFGLTDDQVSGPPSAPAEDR-203
			384-NRPPFGQGYTQPGPGYR-400
a3	TSG101	9	24-ETVNVITLYK-33
			218-DGTISEDTIR-227
			228-ASLISAVSDK-237
			248-AQAELNALK-257
			270-LEEMVTR-276
			294-KDEELSSALEK-304
			295-DEELSSALEK-304
			382-KTAGLSDLY-390
			383-TAGLSDLY-390
a4	VPS37C	2	40-EMALATNR-47
			111-IEEESEAMAEK-121